Efficient embedded cluster density approximation calculations with an orbital-free treatment of environments

Yu-Chieh Chi,[†] Maliheh Shaban Tameh,[‡] and Chen Huang[*,¶]

†*Department of Scientific Computing, Florida State University, Tallahassee, Florida 32306, USA*

‡*Department of Chemistry, University of Minnesota, Minneapolis, Minnesota 55455, USA*

¶*Department of Scientific Computing, Materials Science and Engineering Program, National High Magnetic Field Laboratory, Florida State University, Tallahassee, Florida 32306, USA*

E-mail: chuang3@fsu.edu

Abstract

The computational cost of the Kohn-Sham density functional theory (KS-DFT), employing advanced orbital-based exchange-correlation (XC) functionals, increases quickly for large systems. To tackle this problem, we recently developed a local correlation method in the framework of KS-DFT: the embedded cluster density approximation (ECDA). The aim of ECDA is to obtain accurate electronic structures in the entire system. With ECDA, for each atom in a system, we define a cluster to enclose that atom, with the rest atoms treated as the environment. The system's electron density is then partitioned among the cluster and the environment. The cluster's XC energy density is then calculated based on its electron density using an advanced orbital-based

XC functional. The system's XC energy is obtained by patching all clusters' XC energy densities in an atom-by-atom manner. In our previous formulation of ECDA, environments were treated by KS-DFT, which makes the following two tasks computationally expensive for large systems. The first task is to partition the system's electron density among a cluster and its environment. The second task is to solve the environments' Sternheimer equations for calculating the system's XC potential. In this work, we remove these two computational bottlenecks by treating the environments with the orbital-free (OF) DFT. The new method is called ECDA-envOF. The performance of ECDA-envOF is examined in two systems: ester and Cl-tetracene, for which the exact exchange (EXX) is used as the advanced XC functional. We show that ECDA-envOF gives results that are very close to the previous formulation in which the environments were treated by KS-DFT. Therefore ECDA-envOF can be used for future large-scale simulations. Another focus of this work is to examine ECDA-envOF's performance on systems having different bond types. With ECDA-envOF, we calculate the energy curves for stretching/compressing some covalent, metallic, and ionic systems. ECDA-envOF's predictions agree well with the benchmarks by using reasonably large clusters. These examples demonstrate that ECDA-envOF is nearly a black-box local correlation method for investigating heterogeneous materials in which different bond types exist.

1 Introduction

It is important to obtain accurate electronic structures in large systems. Toward such goal, local correlation methods were actively developed in the past, based on the observation that the Coulomb interactions between electrons quickly decay over distance in many systems.[1–3] A key step for developing local correlation methods is to define locally correlated electrons. Locally correlated electrons can be defined based on the localized molecular orbitals, and methods of this type include the method of increments,[4,5] local configuration interaction method,[6–8] local coupled cluster methods,[9–13] local many-body perturbation theory.[14–18] Lo-

cally correlated electrons can also be defined by partitioning the system's density matrix, which leads to various density-matrix embedding methods.[19–27] Local correlation methods can also be formulated based on Green's function, such as the dynamical mean field theory[28–31] and the self-energy embedding.[32]

Another way to define locally correlated electrons is to partition the electron density. Methods of this type are often called density embedding.[33–49] With density embedding, a system's electron density is partitioned among a cluster and its environment. The cluster's electronic property is then calculated using a high-level quantum mechanical method. Previous density-embedding approaches often focused on obtaining accurate electronic structures in the region of interest. Recently, several density-embedding-based local correlation methods for obtaining accurate electronic structures in the entire system have been developed, such as the many-electron expansion method[48] and the embedded cluster density approximation (ECDA).[50,51]

In this work, we further develop the ECDA method, which is a local correlation method formulated in the framework of Kohn-Sham density functional theory (KS-DFT).[52,53] With ECDA, a system's exchange-correlation (XC) energy is obtained by patching the clusters' XC energy densities that are calculated using advanced, orbital-based XC functionals. The idea of ECDA is illustrated in Figure 1, in which ECDA is applied to benzene. For each atom in the molecule, we define a cluster to enclose it, with the rest atoms considered as its environment. The central atoms of these clusters are marked by red circles, and the clusters are defined by including the nearest neighbors. In Figure 1, each subplot shows the electron densities of a cluster and its associated environment. The density partitioning among a cluster and its environment is carried out using the density functional embedding theory.[44,49] After calculating the clusters' XC energy densities using high-level XC functionals, the clusters' XC energy densities are projected to their central atoms. The system's XC energy is then obtained as the sum of these atomic XC energy densities.

One merit of ECDA is that the system's XC potential can be efficiently calculated,[54]

which makes ECDA a fully self-consistent method. ECDA can therefore be used to investigate systems that have significant charge redistribution (under the assumption that the electron correlations in these systems are local). Furthermore, ECDA is a variational method and its analytical energy gradients can be derived,[51] which makes it possible to efficiently optimize structures and calculate structure-related properties (such as phonon spectra). Different from other local correlation methods that are based on localized molecule orbitals, it is not straightforward for ECDA to use correlated wave function methods as cluster solvers, because clusters often have fractional electron numbers from the density partitioning. However, it is straightforward to solve clusters using advanced orbital-based XC functionals, which makes ECDA a nearly "black-box" local correlation method for scaling up high-level KS-DFT calculations.

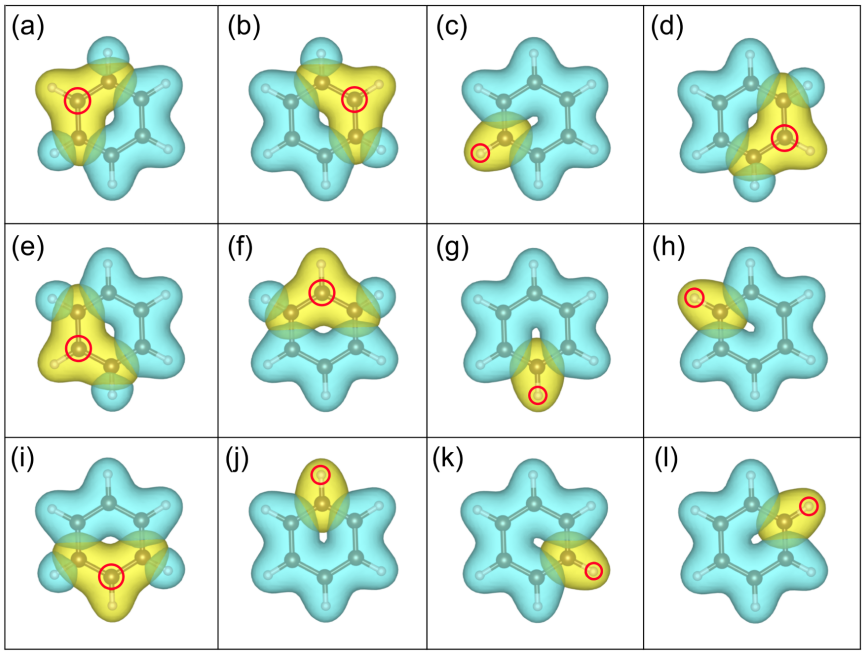

Figure 1: Electron densities of the clusters and their associated environments. Clusters are defined for the central atoms marked by red circles. Cluster electron densities are yellow and environment electron densities are blue. C and H atoms are brown and grey, respectively.

In this work, we overcome several computational bottlenecks in our previous formulation of ECDA. These computational bottlenecks were all due to the KS-DFT treatment of environments. For a large system, environments are large, which makes the following two tasks

computationally expensive. The first task is to solve the environment electron densities for partitioning the system's electron density. The second task is to solve the environments' Sternheimer equations for calculating the system's XC potential. In this work, we remove these computational bottlenecks by treating environments using orbital-free (OF) DFT.[55–58] This new ECDA method is termed ECDA-envOF. The previous formulation (in which the environments were treated by KS-DFT) is termed ECDA-envKS. In this work, we demonstrate that ECDA-envOF and ECDA-envKS give very similar results.

The paper is organized as follows. First, we give an introduction to ECDA. We then discuss how to partition a system's electron density among a cluster and its environment for the case that the environment is treated by either KS-DFT or OF-DFT. To make ECDA-envOF a self-consistent method, we derive the equations for calculating the system's XC potential. Numerical examples are given to demonstrate that ECDA-envOF and ECDA-envKS give very similar results. At last, the performance of ECDA-envOF is examined by calculating the stretching/compressing energies of hydrocarbon molecules, a sodium nanorod, and a MgO nanorod.

2 Theoretical Methods

2.1 Total energy for ECDA

The total energy for ECDA follows that of KS-DFT and is

$$E_{tot} = T_s + J + E_{xc} + E_{ext} + E_{ii} - TS + E_p, \tag{1}$$

where T_s is the KS kinetic energy

$$T_s = -2\sum_j f_j \int \psi_j(\mathbf{r}) \frac{\nabla^2}{2} \psi_j(\mathbf{r}) d^3r. \tag{2}$$

ψ_j is the system's j-th KS orbital and f_j is its occupation number. In Eq. 2, the factor "2" is due to that non-spin-polarized case is considered throughout this work, and the generalization to spin-polarized case is straightforward. J is the Hartree energy

$$J = \iint \frac{\rho_{tot}(\mathbf{r})\rho_{tot}(\mathbf{r}')}{|\mathbf{r}-\mathbf{r}'|} d^3r d^3r', \tag{3}$$

where $\rho_{tot}(\mathbf{r})$ is the system's electron density. E_{xc} is the XC energy which is discussed in Section 2.2. $E_{ext} = \int \rho_{tot}(\mathbf{r}) v_{ext}(\mathbf{r}) d^3r$ is the external energy, with v_{ext} being the system's external potential. E_{ii} is ion-ion Coulomb energy. T is the electronic temperature and S is the electronic entropy

$$S = -2k_B \sum_j [f_j \ln f_j + (1-f_j)\ln(1-f_j)], \tag{4}$$

where k_B is the Boltzmann constant. The reason for having the entropy term is not for considering the temperature but for making the density partitioning (discussed in Section 2.4) numerically stable, as explained in our previous work.[50,59]

E_p in Eq. 1 is a penalty term for regularizing the optimized effective potential (OEP) equation,[60–63] in order to obtain a smooth XC potential as discussed in our previous work.[51] E_p is defined as[51]

$$E_p = \frac{1}{2}\gamma \left[\int d\mathbf{r}' v_d^2(\mathbf{r}') + \int d\mathbf{r}' |\nabla v_d(\mathbf{r}')|^2 \right] \tag{5}$$

with $v_d(\mathbf{r}) = v_s(\mathbf{r}) - v_H(\mathbf{r}) - v_{ext}(\mathbf{r})$. v_s is the system's KS potential, and $v_H = \delta J/\delta\rho_{tot}$ is the Hartree potential. Since the total energy contains E_p, v_d consists of both the XC potential $v_{xc} = \delta E_{xc}/\delta\rho_{tot}$ and the penalty potential $v_p = \delta E_p/\delta\rho_{tot}$. γ controls the weight of the penalty term and is set to 10^{-4} in this work. To make ECDA a self-consistent method, we need to calculate $v_{xc} + v_p$, which is discussed in Section 2.5. The system's KS equation

finally becomes

$$\left[-\frac{1}{2}\nabla^2 + v_{ext}(\mathbf{r}) + v_H(\mathbf{r}) + v_{xc}(\mathbf{r}) + v_p(\mathbf{r})\right]\psi_i(\mathbf{r}) = \epsilon_i\psi_i(\mathbf{r}). \tag{6}$$

2.2 The calculation of the XC energy with ECDA

In this work, the exact exchange (EXX) is used as the high-level XC functional for calculating clusters' XC energy densities. EXX is defined as[64]

$$E_x^{\mathrm{EXX}} = -\sum_k \sum_l f_k c_{kl} \iint d\mathbf{r} d\mathbf{r}' \frac{\varphi_k(\mathbf{r})\varphi_l(\mathbf{r})\varphi_l(\mathbf{r}')\varphi_k(\mathbf{r}')}{|\mathbf{r}-\mathbf{r}'|}, \tag{7}$$

where k and l run over all orbitals. $\{\varphi_k\}$ are the KS orbitals, $\{e_k\}$ are the orbital energies, and $c_{kl} = 1 + \mathrm{sgn}(e_k - e_l)$. EXX defined in Eq. 7 directly follows the adiabatic connection fluctuation-dissipation theorem (ACFDT)[65–68] and is different from the Hartree-Fock theory, as pointed in out in Ref.[64]. The reason for using ACFDT-based EXX is that its exchange holes always satisfy the sum rule, even for systems having fractionally occupied orbitals.[54,69] This is important since clusters defined based on density partitioning often have fractionally occupied KS orbitals. ACFDT-based EXX ensures that the system's XC energy density can be better approximated by clusters' XC energy densities. To patch the system's EXX energy, we need to define the EXX energy density, which is given below

$$\varepsilon_x^{\mathrm{EXX}}(\mathbf{r}) = -\sum_k \sum_l f_k c_{kl} \varphi_k(\mathbf{r})\varphi_l(\mathbf{r}) \int \frac{\varphi_l(\mathbf{r}')\varphi_k(\mathbf{r}')}{|\mathbf{r}-\mathbf{r}'|}, \tag{8}$$

where k and l run over occupied orbitals.

After calculating the clusters' XC energy densities, the system's XC energy is obtained as

$$E_{xc} = \sum_{j=1}^{N_{\mathrm{atom}}} \int w_j(\mathbf{r}) \Delta\varepsilon_{xc}^{clu_j}(\mathbf{r}) d^3r + E_{xc}^{\mathrm{LDA}}[\rho_{tot}] \tag{9}$$

with

$$\Delta\varepsilon_{xc}^{clu_j}(\mathbf{r}) = \varepsilon_{xc,\mathrm{EXX}}^{clu_j}(\mathbf{r}) - \varepsilon_{xc,\mathrm{LDA}}^{clu_j}(\mathbf{r}). \tag{10}$$

$E_{xc}^{\mathrm{LDA}}[\rho_{tot}]$ is the system's XC energy calculated using the local density approximation (LDA).[70] The first term on the right-hand side of Eq. 9 is the correction to $E_{xc}^{\mathrm{LDA}}[\rho_{tot}]$. $w_j(\mathbf{r})$ is the atomic weight function according to Becke's atom-in-molecule scheme (see Ref.[51] for details). $w_j(\mathbf{r})$ projects the cluster j's XC energy density to the central atom j to avoid any boundary effect. In Eq. 10, $\varepsilon_{xc,\mathrm{EXX}}^{clu_j}(\mathbf{r})$ and $\varepsilon_{xc,\mathrm{LDA}}^{clu_j}(\mathbf{r})$ are cluster j's EXX and LDA energy densities, respectively.

2.3 Partition a system's electron density with the environments treated by KS-DFT

The cluster's electron density is obtained by partitioning ρ_{tot} among the cluster and its environment. For the case that both cluster and environment are treated by KS-DFT, the density partitioning was discussed in our previous work.[51] In what follows, we briefly review it and show how to perform the density partitioning for the case that environments are treated by OF-DFT in the next section.

Let's focus on the atom j. We first define the number of electrons in the cluster and the environment as

$$N_{clu_j} = \int w_{clu_j}(\mathbf{r})\rho_{tot}(\mathbf{r})d^3r \tag{11}$$

$$N_{env_j} = \int w_{env_j}(\mathbf{r})\rho_{tot}(\mathbf{r})d^3r, \tag{12}$$

where $w_{clu_j} = \sum_k w_k$ (k loops over all atoms in the cluster) and $w_{env_j} = 1 - w_{clu_j}$ are the weight functions for the cluster and the environment, respectively. We then partition the

system's KS potential among the cluster and the environment as

$$v_{clu_j}(\mathbf{r}) = (v_s(\mathbf{r}) - \mu - v_b)w_{clu_j}(\mathbf{r}) \tag{13}$$

$$v_{env_j}(\mathbf{r}) = (v_s(\mathbf{r}) - \mu - v_b)w_{env_j}(\mathbf{r}), \tag{14}$$

where μ is the system's chemical potential. The term $v_s - \mu$ ensures that the system's chemical potential is shifted to zero at distant. By subtracting v_b, $v_{clu_j}(\mathbf{r})$ and $v_{env_j}(\mathbf{r})$ are further decreased to make sure that the electrons are well confined in the cluster and the environment. ECDA results are not sensitive to the choice of v_b, and v_b is set to 0.5 a.u. in this work.

An embedding potential (v_{emb_j}) is then added to both $v_{clu_j}(\mathbf{r})$ and $v_{env_j}(\mathbf{r})$ as

$$v_s^{clu_j}(\mathbf{r}) = v_{clu_j}(\mathbf{r}) + v_{emb_j}(\mathbf{r}) \tag{15}$$

$$v_s^{env_j}(\mathbf{r}) = v_{env_j}(\mathbf{r}) + v_{emb_j}(\mathbf{r}). \tag{16}$$

The cluster and environment's electron densities are obtained by solving their KS equations

$$\left(-\frac{1}{2}\nabla^2 + v_s^{clu_j}(\mathbf{r})\right)\phi_i^{clu_j}(\mathbf{r}) = \epsilon_i^{clu_j}\phi_i^{clu_j}(\mathbf{r}) \tag{17}$$

$$\left(-\frac{1}{2}\nabla^2 + v_s^{env_j}(\mathbf{r})\right)\phi_i^{env_j}(\mathbf{r}) = \epsilon_i^{env_j}\phi_i^{env_j}(\mathbf{r}), \tag{18}$$

where $\phi_i^{clu_j}$ and $\phi_i^{env_j}$ are the i-th KS orbitals of the cluster and the environment, respectively. $\epsilon_i^{clu_j}$ and $\epsilon_i^{env_j}$ are the i-th orbital energies of the cluster and the environment, respectively. The cluster and the environment's electron densities are

$$\rho_{clu_j}(\mathbf{r}) = 2\sum_i f_i^{clu_j}[\phi_i^{clu_j}(\mathbf{r})]^2 \tag{19}$$

$$\rho_{env_j}(\mathbf{r}) = 2\sum_i f_i^{env_j}[\phi_i^{env_j}(\mathbf{r})]^2, \tag{20}$$

where $f_i^{clu_j}$ and $f_i^{env_j}$ are the occupation numbers of the cluster and environment, respectively. v_{emb_j} is determined by making the density-matching condition to hold

$$\rho_{clu_j}(\mathbf{r}) + \rho_{env_j}(\mathbf{r}) = \rho_{tot}(\mathbf{r}). \tag{21}$$

In our previous work, $v_{emb_j}(\mathbf{r})$ was solved using a modified Zhao-Parr method.[51] Solving v_{emb_j} is an OEP problem, which needs to be regularized for obtaining a smooth solution. The regularization leads to an approximate density-matching condition (Eq. 33) that is different from Eq. 21. See Ref.[51] for details.

2.4 Partition a system's electron density with the environments treated by OF-DFT

Next, we discuss how to modify the above density-partitioning scheme for the case that environments are treated by OF-DFT. For the kinetic energy density functional (KEDF), we use the linear combination of a modified Thomas-Fermi[71,72] (denoted as TFm) functional and a modified von Weizsäcker[73] (denoted as vWm) functional:

$$T_s \approx T_{\mathrm{TFm}} + \lambda T_{\mathrm{vWm}} \tag{22}$$

with TFm and vWm KEDFs defined as

$$T_{\mathrm{TFm}} = C_{\mathrm{TF}} \int F(\mathbf{r}) \rho(\mathbf{r})^{5/3} d^3r \tag{23}$$

$$T_{\mathrm{vWm}} = \int \phi_{\mathrm{m}}(\mathbf{r}) \left(-\frac{1}{2}\nabla^2 \right) \phi_{\mathrm{m}}(\mathbf{r}) d^3r \tag{24}$$

with $C_{\mathrm{TF}} = \frac{3}{10}(3\pi^2)^{2/3}$, $F(\mathbf{r}) = 1 - \exp\left[-(\rho(\mathbf{r})/\rho_0)^{1/3}\right]$, and $\phi_{\mathrm{m}}(\mathbf{r}) = \sqrt{\rho(\mathbf{r}) + \rho_0}$. By using F, the inverse of the TFm kernel ($K_{\mathrm{TFm}}(\mathbf{r}, \mathbf{r}') = \delta^2 T_{\mathrm{TFm}} / \delta\rho(\mathbf{r})\delta\rho(\mathbf{r}')$) does not diverge in low electron-density regions. ϕ_{m} is used to ensure that the vWm potential ($v_{\mathrm{vWm}}(\mathbf{r}) =$

$\delta T_{\mathrm{vWm}}/\delta\rho(\mathbf{r})$) does not diverge in low electron-density regions. The reason for a possible divergence is that it is difficult to solve $\rho(\mathbf{r})$ accurately in low-density regions using plane-wave basis (which is used in this work). We set $\rho_0 = 10^{-5}$ a.u. in both F and ϕ_m in this work.

Since environments are treated by OF-DFT, v_s in Eq. 14 needs to be replaced by its OF-DFT counterpart v_{OF}:

$$v_{\mathrm{OF}}(\mathbf{r}) = \mu - \frac{\delta T_{\mathrm{TFm}}[\rho_{tot}]}{\delta\rho_{tot}(\mathbf{r})} - \lambda\frac{\delta T_{\mathrm{vWm}}[\rho_{tot}]}{\delta\rho_{tot}(\mathbf{r})}. \tag{25}$$

Using v_{OF}, Eq. 16 becomes

$$v_{\mathrm{OF}}^{env_j}(\mathbf{r}) = (v_{\mathrm{OF}}(\mathbf{r}) - \mu - v_b)w_{env_j}(\mathbf{r}) + v_{emb_j}(\mathbf{r}). \tag{26}$$

To partition the system's electron density among the cluster and its environment, we still employ the Zhao-Parr method developed in our previous work.[51] The only change is that now the environment is treated by OF-DFT. We drop the subscript j in the following discussions for simplicity. The Zhao-Parr energy is defined as[74,75]

$$E_{\mathrm{zp}} = E_{clu} + E_{env}^{\mathrm{OF}} + \frac{\eta}{2}\iint e^{\alpha|\mathbf{r}-\mathbf{r}'|}\frac{\Delta\rho(\mathbf{r})\Delta\rho(\mathbf{r}')}{|\mathbf{r}-\mathbf{r}'|}d^3r d^3r' \tag{27}$$

with $\Delta\rho = \rho_{clu}+\rho_{env}-\rho_{tot}$. The last term is the penalty term to enforce the density-matching condition. The penalty term is defined based on the Yukawa potential in order to regularize the equations for solving the system's XC potential as explained in Ref.[51] α is set to 0.2 bohr^{-1} in this work. η controls how good the density-matching condition is satisfied. In practice, results (such as total energies) need to be converged with respect to η. In Eq. 27,

E_{clu} and E_{env}^{OF} are the cluster and environment's energies defined as

$$\begin{aligned} E_{clu} &= 2\sum_k f_k^{clu} \int \phi_k^{clu}(\mathbf{r}) \left(-\frac{1}{2}\nabla^2\right) \phi_k^{clu}(\mathbf{r}) d^3r \\ &\quad + \int v_{clu}(\mathbf{r})\rho_{clu}(\mathbf{r}) dr^3 - TS_{clu} \end{aligned} \tag{28}$$

$$E_{env}^{\mathrm{OF}} = T_{\mathrm{TFm}}[\rho_{env}] + \lambda T_{\mathrm{vWm}}[\rho_{env}] + \int v_{\mathrm{OF}}^{env}(\mathbf{r})\rho_{env}(\mathbf{r}) d^3r \tag{29}$$

where T is the smearing temperature used in the Fermi-Dirac statistics for assigning the occupation numbers of the cluster's KS orbitals. To be consistent with the total system, T is the same as the smearing temperature used in Eq. 1. S_{clu} is the cluster's electronic entropy. By minimizing E_{zp} against the cluster's KS orbitals, we obtain the KS equations for the cluster:

$$\left(-\frac{1}{2}\nabla^2 + v_{clu}(\mathbf{r}) + v_{pen}(\mathbf{r})\right) \phi_k^{clu}(\mathbf{r}) = e_k^{clu}\phi_k^{clu}(\mathbf{r}) \tag{30}$$

where $\phi_k^{clu}(\mathbf{r})$ and e_k^{clu} are the k^{th} KS orbital and orbital energy. In Eq. 30, v_{pen} is due to the penalty term and is

$$v_{pen}(\mathbf{r}) = \eta \int e^{-\alpha|\mathbf{r}-\mathbf{r}'|} \frac{\Delta\rho(\mathbf{r}')}{|\mathbf{r}-\mathbf{r}'|} d^3r'. \tag{31}$$

For the case that an environment is treated by the TFm+λvWm KEDF, the environment's electron density ρ_{env} is solved by directly minimizing E_{zp} against ρ_{env} with the cluster's electron density fixed. This leads to minimizing the following energy against ρ_{env}

$$E_{env}^{\mathrm{OF}'} = E_{env}^{\mathrm{OF}} + \int v_{pen}(\mathbf{r})\rho_{env}(\mathbf{r}) d^3r. \tag{32}$$

For the case that an environment is treated by the TFm KEDF, ρ_{env} is calculated by solving a modified TF equation.

In summary, the density partitioning is performed with the following steps. For a given v_{pen}, Eq. 30 is solved to obtain ρ_{clu}, and $E_{env}^{\mathrm{OF}'}$ is minimized to obtain ρ_{env}. v_{pen} is then updated using Eq. 31. These steps are repeated until the convergence of v_{pen} is reached.

The convergence is accelerated by using the Pulay mixing.[76] At convergence, v_{pen} is taken as the embedding potential. Note that the density-matching condition Eq. 21 can only be reproduced for $\eta \to \infty$. For a finite η, Eq. 21 should be replaced by the following condition:[51]

$$\rho_{tot}(\mathbf{r}) = \rho_{clu}(\mathbf{r}) + \rho_{env}(\mathbf{r}) - \frac{\alpha^2 - \nabla^2}{4\pi\eta} v_{emb}(\mathbf{r}). \tag{33}$$

This new density-matching condition is important for deriving the XC potential in Section 2.6, since it connects ρ_{clu} with ρ_{tot}.

2.5 The calculation of the XC potential with ECDA

To make ECDA a self-consistent method, next we derive the system's XC potential. We actually calculate the sum $v_{xcp} = v_{xc} + v_p$ by solving the following OEP equation

$$\frac{\delta(E_{xc} + E_p)}{\delta v_s(\mathbf{r})} = \int v_{xcp}(\mathbf{r}')\chi_0(\mathbf{r}, \mathbf{r}')d^3r', \tag{34}$$

where $\chi_0(\mathbf{r}, \mathbf{r}') = \delta\rho(\mathbf{r})/\delta v_s(\mathbf{r}')$ is the system's KS linear response function. The key is to calculate the left-hand side of Eq. 34. For the case that the environments are treated by KS-DFT, the calculations of $\delta E_p/\delta v_s$ and $\delta E_{xc}/\delta v_s$ were discussed in Ref.[51] In what follows we discuss how to calculate $\delta E_{xc}/\delta v_s$ for the case that the environments are treated by OF-DFT.

Since the cluster i's XC energy density depends on N_{clu_j} and $v_s^{clu_j}$, we have

$$\frac{\delta E_{xc}}{\delta v_s(\mathbf{r})} = \sum_{j=1}^{N_{\text{atom}}} \left[p_{1,j}(\mathbf{r}) + p_{2,j}(\mathbf{r}) + p_{3,j}(\mathbf{r})\right], \tag{35}$$

with

$$p_{1,j}(\mathbf{r}) = \int y_j(\mathbf{r}') \frac{\delta v_s^{clu_j}(\mathbf{r}')}{\delta v_s(\mathbf{r})} d^3r' \tag{36}$$

$$p_{2,j}(\mathbf{r}) = \int w_j(\mathbf{r}') \frac{\partial \Delta\varepsilon_{xc,j}(\mathbf{r}')}{\partial N_{clu_j}}\bigg|_{v_s^{clu_j}} \frac{\delta N_{clu_j}}{\delta v_s(\mathbf{r})} d^3r' \tag{37}$$

$$p_{3,j}(\mathbf{r}) = \int w_j(\mathbf{r}') v_{xc}^{\mathrm{LDA}}(\mathbf{r}') \chi_0(\mathbf{r}, \mathbf{r}') d^3r', \tag{38}$$

where v_{xc}^{LDA} is the system's LDA XC potential and y_j is defined as

$$y_j(\mathbf{r}') = \int w_j(\mathbf{r}) \frac{\delta \Delta\varepsilon_{xc,j}(\mathbf{r})}{\delta v_s^{clu,j}(\mathbf{r}')}\bigg|_{N_{clu_j}} d^3r. \tag{39}$$

If the employed XC functional is an explicit function of KS orbitals (such as EXX functional used here), y_i can be calculated following the chain rule as

$$y_j(\mathbf{r}') = \sum_k \iint w_j(\mathbf{r}) \frac{\delta \Delta\varepsilon_{xc,j}(\mathbf{r})}{\delta \phi_k^{clu_j}(\mathbf{r}_1)} \frac{\delta \phi_k^{clu_j}(\mathbf{r}_1)}{\delta v_s^{clu,j}(\mathbf{r}')}\bigg|_{N_{clu_j}} d\mathbf{r}_1 d\mathbf{r}, \tag{40}$$

where k runs over all orbitals in the cluster j. For EXX, y_j has been derived in Ref.[54] The calculations of $p_{2,j}$ and $p_{3,j}$ do not depend on how environments are treated and follow our previous discussions.[51]

The calculation of $p_{1,j}$ depends on how the environments are treated. For simplicity, we drop the subscript j in the following derivations. p_1 depends on $\delta v_s^{clu}/\delta v_s$, which is given by (based on Eqs. 13 and 15)

$$\frac{\delta v_s^{clu}(\mathbf{r}')}{\delta v_s(\mathbf{r})} = \left[\delta(\mathbf{r}' - \mathbf{r}) - \frac{\delta\mu}{\delta v_s(\mathbf{r})}\right] w_{clu}(\mathbf{r}') + \frac{\delta v_{emb}(\mathbf{r}')}{\delta v_s(\mathbf{r})}. \tag{41}$$

Above, $\delta\mu/\delta v_s(\mathbf{r})$ is calculated as $\delta\mu/\delta v_s(\mathbf{r}) = \sum_k \psi_k^2(\mathbf{r}) \partial\mu/\partial e_k$, where e_k is the orbital energy of the k-th orbital and $\partial\mu/\partial e_k = f_k(1-f_k)/\sum_m f_m(1-f_m)$. The calculation of $\delta v_{emb}/\delta v_s$ is given in the next section.

2.6 The calculation of $\delta v_{emb}(\mathbf{r})/\delta v_s(\mathbf{r}')$

The key for deriving the system's XC potential is to derive the dependence of the embedding potential on the system's KS potential, which can be derived based on the density-matching condition (Eq. 33). By perturbing v_s, Eq. 33 can be linearized to

$$\delta\rho_{tot}(\mathbf{r}) = \delta\rho_{clu}(\mathbf{r}) + \delta\rho_{env}(\mathbf{r}) - \frac{\alpha^2 - \nabla^2}{4\pi\eta}\delta v_{emb}(\mathbf{r}), \tag{42}$$

with

$$\delta\rho_{tot}(\mathbf{r}) = \int \chi_0(\mathbf{r},\mathbf{r}')\delta v_s(\mathbf{r}')d^3r'. \tag{43}$$

$$\delta\rho_{clu}(\mathbf{r}) = \int \chi_0^{clu}(\mathbf{r},\mathbf{r}')\delta v_s^{clu}(\mathbf{r}')d^3r' + \left.\frac{\partial\rho_{clu}(\mathbf{r})}{\partial N_{clu}}\right|_{v_s^{clu}}\delta N_{clu} \tag{44}$$

$$\delta\rho_{env}(\mathbf{r}) = \int \chi_{\mathrm{OF}}^{env}(\mathbf{r},\mathbf{r}')\delta v_{\mathrm{OF}}^{env}(\mathbf{r}')d^3r' + \left.\frac{\partial\rho_{env}(\mathbf{r})}{\partial N_{env}}\right|_{v_{\mathrm{OF}}^{env}}\delta N_{env}, \tag{45}$$

where $\chi_{\mathrm{OF}}^{env}(\mathbf{r},\mathbf{r}') = \delta\rho_{env}(\mathbf{r}')/\delta v_{\mathrm{OF}}^{env}(\mathbf{r})$ is the OF linear response function for the environment. δv_s^{clu} and $\delta v_{\mathrm{OF}}^{env}$ are

$$\delta v_s^{clu}(\mathbf{r}) = w_{clu}(\mathbf{r})(\delta v_s(\mathbf{r}) - \delta\mu) + \delta v_{emb}(\mathbf{r}) \tag{46}$$

$$\delta v_{\mathrm{OF}}^{env}(\mathbf{r}) = w_{env}(\mathbf{r})(\delta v_{\mathrm{OF}}(\mathbf{r}) - \delta\mu) + \delta v_{emb}(\mathbf{r}). \tag{47}$$

The connection between δv_{OF} and δv_s is

$$\begin{aligned}\frac{\delta v_{\mathrm{OF}}(\mathbf{r}')}{\delta v_s(\mathbf{r})} &= \int \frac{\delta v_{\mathrm{OF}}(\mathbf{r}')}{\delta\rho_{tot}(\mathbf{r}_1)}\frac{\delta\rho_{tot}(\mathbf{r}_1)}{\delta v_s(\mathbf{r})}d^3r_1 \\ &= \int \chi_{\mathrm{OF}}^{-1}(\mathbf{r}',\mathbf{r}_1)\chi_0(\mathbf{r}_1,\mathbf{r})d^3r_1,\end{aligned} \tag{48}$$

where $\chi_{\rm OF}(\mathbf{r},\mathbf{r}') = \delta\rho_{tot}(\mathbf{r})/\delta v_{\rm OF}(\mathbf{r}')$ is the system's OF linear response function. δN_{clu} and δN_{env} depend on δv_s as

$$\frac{\delta N_{clu}}{\delta v_s(\mathbf{r})} = \int \chi_0(\mathbf{r},\mathbf{r}') w_{clu}(\mathbf{r}') d^3r' \tag{49}$$

$$\frac{\delta N_{env}}{\delta v_s(\mathbf{r})} = \int \chi_0(\mathbf{r},\mathbf{r}') w_{env}(\mathbf{r}') d^3r'. \tag{50}$$

After writing everything in terms on δv_s, we insert Eqs. 43, 44, 45, 49, and 50 into Eq. 42 and obtain

$$\frac{\delta v_{emb}(\mathbf{r}')}{\delta v_s(\mathbf{r})} = \int Q_1^{-1}(\mathbf{r}',\mathbf{r}'') Q_2(\mathbf{r}'',\mathbf{r}) d^3r'', \tag{51}$$

in which Q_1 and Q_2 are (in the matrix presentation)

$$Q_1 = X_0^{clu} + X_{\rm OF}^{env} - \frac{1}{4\pi\eta}(\alpha^2 - \nabla^2) \tag{52}$$

$$\begin{aligned} Q_2 = {} & X_0 - X_0^{clu} W_{clu} - X_{\rm OF}^{env} W_{env} X_{\rm OF}^{-1} X_0 \\ & + [X_0^{clu}|w_{clu}\rangle + X_{\rm OF}^{env}\,|w_{env}\rangle]\,\langle \frac{\delta\mu}{\delta v_s}| \\ & - \left[|\frac{\partial\rho_{clu}}{\partial N_{clu}}\rangle\,\langle w_{clu}| + |\frac{\partial\rho_{env}}{\partial N_{env}}\rangle\,\langle w_{env}| \right] X_0. \end{aligned} \tag{53}$$

where X_0^{clu}, X_0^{env}, and X_0 are matrix representations of the KS linear responses of the cluster, environment, and total system, respectively. $X_{\rm OF}^{env}$ and $X_{\rm OF}$ are the matrix representation of the OF linear responses of the environment and total system, respectively. In real space, W_{clu} and W_{env} are diagonal matrices whose diagonal elements are the cluster and environment's weight functions, respectively. For the case that the environments are treated by TFm KEDF, $\partial\rho_{env}/\partial N_{env}$ in Eq. 53 is calculated using the central finite difference method by changing N_{env} by 0.001. For the case that environments are treated by vWm KEDF, $\partial\rho_{env}/\partial N_{env}$ is calculated following Appendix C.

Combining Eqs. 51, 41, and 36, the expression for p_1 is

$$\begin{aligned} p_1(\mathbf{r}) &= y(\mathbf{r})w_{clu}(\mathbf{r}) + \int Q_2^T(\mathbf{r},\mathbf{r}')z(\mathbf{r}')d^3r' \\ &\quad -\frac{\delta\mu}{\delta v_s(\mathbf{r})}\int y(\mathbf{r}')w_{clu}(\mathbf{r}')d^3r', \end{aligned} \tag{54}$$

in which z is defined

$$z(\mathbf{r}) = \int Q_1^{-1}(\mathbf{r},\mathbf{r}')y(\mathbf{r}')d^3r'. \tag{55}$$

To avoid inverting Q_1, in practice z is obtained by solving the linear equation

$$\int Q_1(\mathbf{r},\mathbf{r}')z(\mathbf{r}')d^3r' = y(\mathbf{r}) \tag{56}$$

using the conjugate gradient method. Eqs. 54 and 56 involve calculating the products between KS and OF linear response functions and vectors. The product between KS linear response and a vector is calculated by solving the Sternheimer equation derived for systems having fractionally occupied KS orbitals.[77–79] The product between OF linear response and a vector is calculated following the methods given in Appendices A and B. When applying Q_2^T to z in Eq. 54, we need to calculate the product between X_{OF}^{-1} and a vector. For TFm KEDF, X_{OF}^{-1} is the kernel of TFm KEDF: $X_{\mathrm{OF}}^{-1} = K_{\mathrm{TFm}} = \delta^2 T_{\mathrm{TFm}}/\delta\rho(\mathbf{r})\delta\rho(\mathbf{r}')$. For TFm+$\lambda$vWm KEDF, $X_{\mathrm{OF}}^{-1}(\mathbf{r},\mathbf{r}') = K_{\mathrm{TFm}} + \lambda K_{\mathrm{vWm}}$, with $K_{\mathrm{vWm}}(\mathbf{r},\mathbf{r}') = \delta^2 T_{\mathrm{vWm}}/\delta\rho(\mathbf{r})\delta\rho(\mathbf{r}')$.

2.7 Flowchart for ECDA-envOF calculations

To summarize, the flowchart for performing ECDA-envOF calculations is given below.

1. For a given v_s, solve the system's KS equation and obtain its electron density ρ_{tot}.

2. For each atom, partition ρ_{tot} among its cluster and the environment following Section 2.4.

3. Calculate the clusters' XC energy densities and assemble the system's XC energy ac-

cording to Eq. 9. Calculate $\delta E_{xc}/\delta v_s(\mathbf{r})$ following Section 2.5, and calculate $\delta E_p/\delta v_s$ follows Ref.[51]. Solve the OEP Eq. 34 to obtain $v_{xc} + v_p$.

4. Calculate the system's Hartree potential. Update the system's KS potential as $v_s = v_H + v_{xc} + v_p + v_{ext}$. Check the convergence of v_s. If v_s is converged, exit ECDA calculations. If v_s is not converged, return to Step 1. The convergence of v_s is accelerated using the Pulay mixing.[76]

3 Numerical details

All ECDA and KS-DFT-EXX calculations are implemented in a FORTRAN90 program which calls a modified ABINIT program[80] (version 7.10.4) that solves the KS equation for a given KS potential. To avoid the singularity from the Coulomb potential, EXX energy are calculated in the real space using a Poisson solver[81] implemented in ABINIT. A Fermi-Dirac smearing of 0.1 eV is used for all ECDA and KS-DFT calculations. Molecular structures and EXX potentials are plotted using the VESTA program.[82]

For ester and Cl-tetracene, a relatively small kinetic energy cutoff, 600 eV, is used for all calculations, in order to reduce the cost of EXX calculations and the Sternheimer equation calculations. $\eta = 200$ is used for the electron density partitioning. Troullier-Martins norm-conserving pseudopotentials[83] are used to represent atoms.

For $C_{10}H_2$, $C_{12}H_{14}$, and $C_{12}H_{26}$, a kinetic energy cutoff of 400 eV is used for KS-DFT-EXX and ECDA-envOF(TF) calculations, and $\eta = 5000$ is used for electron density partitioning. Troullier-Martins pseudopotentials are used. The molecules' structures mainly follow Ref.[84] For $C_{10}H_2$, C-H bond is 1.091 Å, C-C triple bond is 1.263 Å, and C-C single bond is 1.320 Å. For $C_{12}H_{14}$, C-H bond is 1.091 Å, C-C single bond is 1.462 Å, C-C double bond is 1.369 Å, C=C-C angle 124.5°, C=C-H angle (inside the chain) is 118.3°, and C=C-H angle (at the two ends of the chain) is 121.7°. For $C_{12}H_{26}$, C-C bond is 1.534 Å, and C-C-C angle is 113.7°. For the H atoms inside the chain, C-H bond is 1.10 Å, and H-C-H angle is

106.1°. The coordinates of the six H atoms at the two ends of the chain are optimized using NWChem program (version 6.8).[85] During the optimization, all other atoms are fixed. The geometry optimization is performed using the Becke, 3-parameter, Lee–Yang–Parr (B3LYP) XC functional[86] and 6-311G** basis set.

The Na nanorod is built from the body-centered cubic Na bulk with a lattice parameter of 4.282 Å. The MgO nanorod is built from the cubic MgO bulk with a lattice constant of 4.217 Å. Their structures are shown in Figure 10. These nanorods are centered in large unit cells, with the distance between periodic images to be 10 Å in all directions. Na and Mg's norm-conserving pseudopotentials[87] are generated using the fhi98PP program.[88] Since the current formalism of ECDA does not support the nonlinear core correction,[89] these pseudopotentials do not have the nonlinear core correction. The pseudopotentials are generated for the ground states of the atoms. Na and Mg's pseudopotentials are generated using Hamann[90] and Troullier-Martins[83] schemes, respectively. The s and p angular momentum channels are used as the local potentials for Na and Mg, respectively. To reduce computational cost, kinetic energy cutoffs of 50 eV and 300 eV are used for the Na and MgO nanorods, respectively. For the Na nanorod, $\eta = 200$ is used for the electron density partitioning. For the MgO nanorod, the Zhao-Parr method is unable to converge due to the charge sloshing of the sum of the cluster and environment's electron densities.[91] The reason is that atoms in ionic systems are far from charge neutral. Therefore, $\rho_{clu}(\mathbf{r}) + \rho_{env}(\mathbf{r}) - \rho_{tot}(\mathbf{r})$ can produce large embedding potential at small wave vectors, due to the attenuated Coulomb potential in the Yukawa function. To avoid such problem, we replace the Yukawa function with $\frac{1}{2}\eta \int (\rho_{clu}(\mathbf{r}') + \rho_{env}(\mathbf{r}') - \rho_{tot}(\mathbf{r}'))^2 d^3r'$ (with $\eta = 2000$), which leads to smooth convergences.

4 Results and discussion

In what follows, ECDA calculations with environments treated by KS-DFT are denoted by ECDA-envKS. ECDA calculations with environments treated by OF-DFT are denoted by

ECDA-envOF. ECDA-envOF calculations with environments treated by TFm KEDF are denoted by ECDA-envOF(TF). ECDA-envOF calculations with environments treated by TFm+$\frac{1}{9}$vWm are denoted by ECDA-envOF(TF+$\frac{1}{9}$vW).

4.1 Compare ECDA-envKS with ECDA-envOF

The comparison between ECDA-envKS and ECDA-envOF is made on two systems: ester and Cl-tetracene, with their structures given in Fig. 2. In Table 1, we compare the total energies from ECDA-envKS and ECDA-envOF calculations. All calculations are self-consistent. Three different cluster sizes are considered: $N_b = 1$, 2, and 3, which indicates that the first, second, and third nearest neighbors are included for defining clusters, respectively. For ECDA-envOF calculations, environments are treated by two different KEDFs: TF and TF+$\frac{1}{9}$vW. Table 1 shows that ECDA-envOF(TF), ECDA-envOF(TF+$\frac{1}{9}$vW), and ECDA-envKS give similar results. As N_b increases, ECDA results gradually converge to KS-DFT-EXX results. Table 2 shows the dipole moments of the two molecules. We have similar observations: ECDA-envKS and ECDA-envOF give similar results, and also ECDA results gradually converge to KS-DFT-EXX results for large N_b.

The good agreement between ECDA-envKS, ECDA-envOF(TF), and ECDA-envOF(TF+$\frac{1}{9}$vW) is due the fact that they give similar cluster electron densities. Taking Cl-tetracene as an example, Figure 3 shows the cluster densities for a specific cluster calculated with the environment treated in different ways. Even though the three cluster densities are slightly different at the cluster-environment boundaries, they are nearly the same inside the cluster. On the other hand, we only consider the XC energy density around the central atom (marked by the red circles in Figure 3), when constructing the system's XC energy with Eq. 9. This largely removes the boundary effect caused by the different treatments for the environments. As a result, the system's XC energy has a weak dependence on how the environments are treated.

Above observation suggests that ECDA-envKS can be replaced by ECDA-envOF in

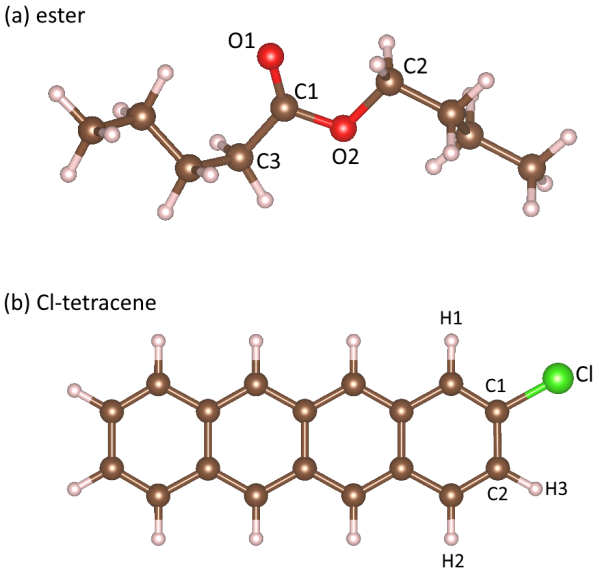

Figure 2: Structures of (a) ester and (b) Cl-tetracene. Oxygen, carbon, hydrogen, and chlorine atoms are red, brown, grey, and green.

Table 1: Total energies (in Hartree) from self-consistent ECDA-envKS and self-consistent ECDA-envOF calculations for ester and Cl-tetracene.

	ester	Cl-tetracene
$N_b = 1$		
ECDA-envKS	-91.587	-120.634
ECDA-envOF(TF)	-91.580	-120.640
ECDA-envOF(TF+$\frac{1}{9}$vW)	-91.581	-120.637
$N_b = 2$		
ECDA-envKS	-91.423	-120.566
ECDA-envOF(TF)	-91.421	-120.569
ECDA-envOF(TF+$\frac{1}{9}$vW)	-91.421	-120.568
$N_b = 3$		
ECDA-envKS	-91.474	-120.543
ECDA-envOF(TF)	-91.474	-120.543
ECDA-envOF(TF+$\frac{1}{9}$vW)	-91.475	-120.542
KS-DFT-EXX	-91.484	-120.553

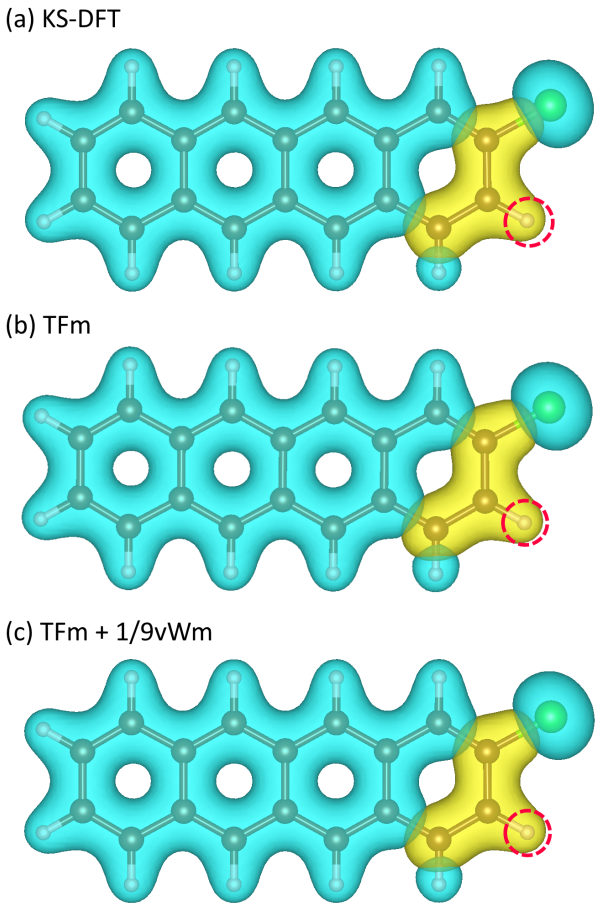

Figure 3: The cluster (yellow) and environment (blue) electron densities from treating the environment using KS-DFT, TFm, and TFm+1/9vWm, respectively. The clusters are defined for the central atoms (marked by the red circles) with $N_b = 2$.

Table 2: Dipoles (in Debye) from self-consistent ECDA-envKS and self-consistent ECDA-envOF calculations for ester and Cl-tetracene.

	ester	Cl-tetracene
$N_b = 1$		
ECDA-envKS	1.68	2.68
ECDA-envOF(TF)	1.70	2.87
ECDA-envOF(TF+$\frac{1}{9}$vW)	1.72	2.86
$N_b = 2$		
ECDA-envKS	1.98	2.19
ECDA-envOF(TF)	1.93	2.30
ECDA-envOF(TF+$\frac{1}{9}$vW)	1.97	2.26
$N_b = 3$		
ECDA-envKS	1.94	2.53
ECDA-envOF(TF)	1.90	2.57
ECDA-envOF(TF+$\frac{1}{9}$vW)	1.96	2.52
KS-DFT-EXX	1.91	2.58

future ECDA calculations. In addition, the good agreement between ECDA-envOF(TF) and ECDA-envOF(TF+$\frac{1}{9}$vW) results suggests that we can use TFm KEDF to treat environments, which is computationally much cheaper than treating the environment with TFm+$\frac{1}{9}$vWm, due to the fact that the TF equation is easy to solve.

To further examine the performance of ECDA-envOF(TF), in Figures 4 and 5 we compare the EXX potentials from self-consistent ECDA-envOF(TF) and self-consistent KS-DFT-EXX calculations. Even for $N_b = 1$, a good agreement between ECDA-envOF(OF) and KS-DFT-EXX is observed. We observe that ECDA-envOF(OF)'s EXX potentials become closer to the KS-DFT-EXX results as N_b increases.

The quality of the EXX potentials predicted by ECDA-envOF(TF) can be assessed by examining the KS eigenvalues shown in Fig. 6. As N_b increases, ECDA-envOF(TF)'s eigenvalues become closer to KS-DFT-EXX's eigenvalues for the occupied orbitals. For the unoccupied orbitals, the convergence is not very good, which may be due to the fact that EXX functional does not depend on the unoccupied orbitals. We expect that the convergence can

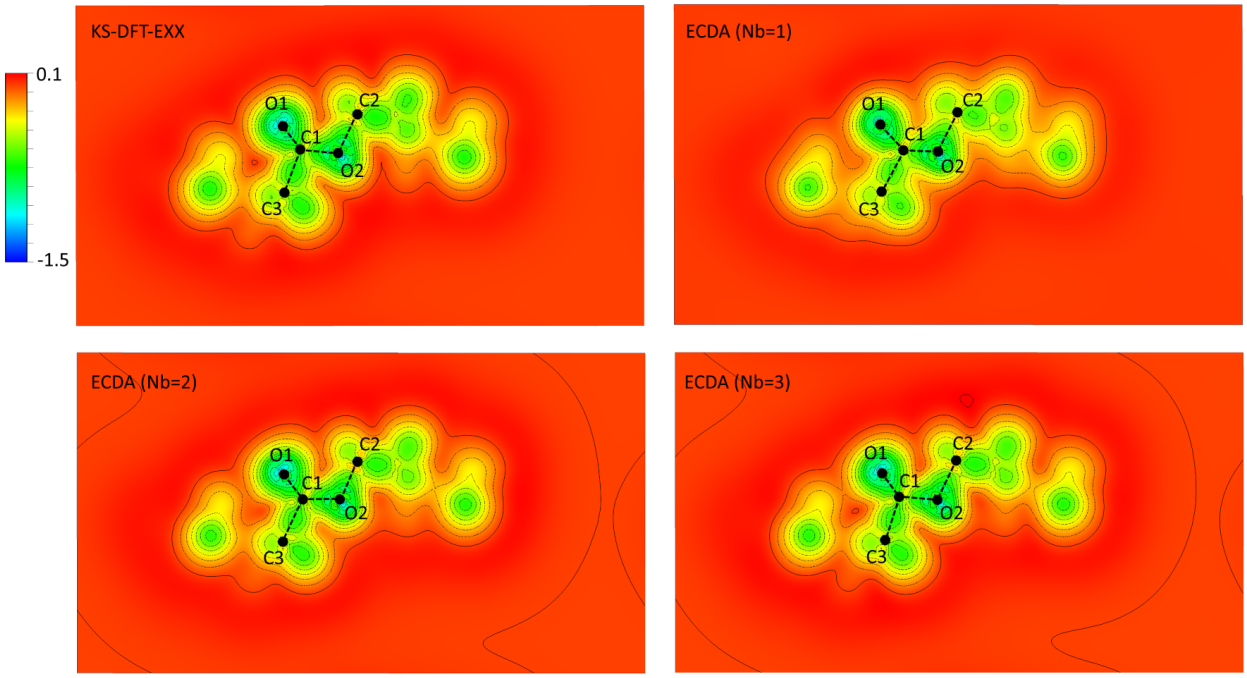

Figure 4: EXX potentials of ester from self-consistent KS-DFT-EXX and self-consistent ECDA-envOF(TF) calculations, with different cluster sizes. Contour plane is defined by the O1, O2 and C1 atoms in Fig. 2(a). Interval between contour lines is 0.1 a.u..

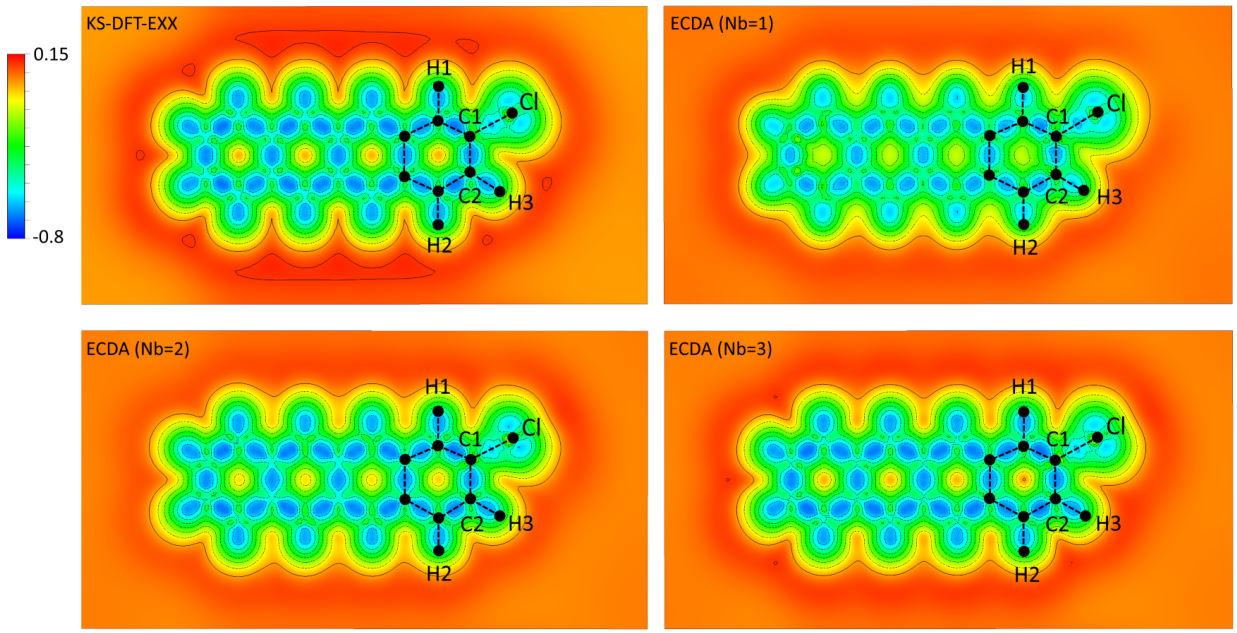

Figure 5: EXX potentials of Cl-tetracene from self-consistent KS-DFT-EXX and self-consistent ECDA-envOF(TF) calculations, with difference cluster sizes. Contour plane is defined by the benzene rings in Fig. 2(b). Interval between contour lines is 0.1 a.u..

be improved, if ECDA calculations employ a correlation energy functional that depends on the unoccupied orbitals.

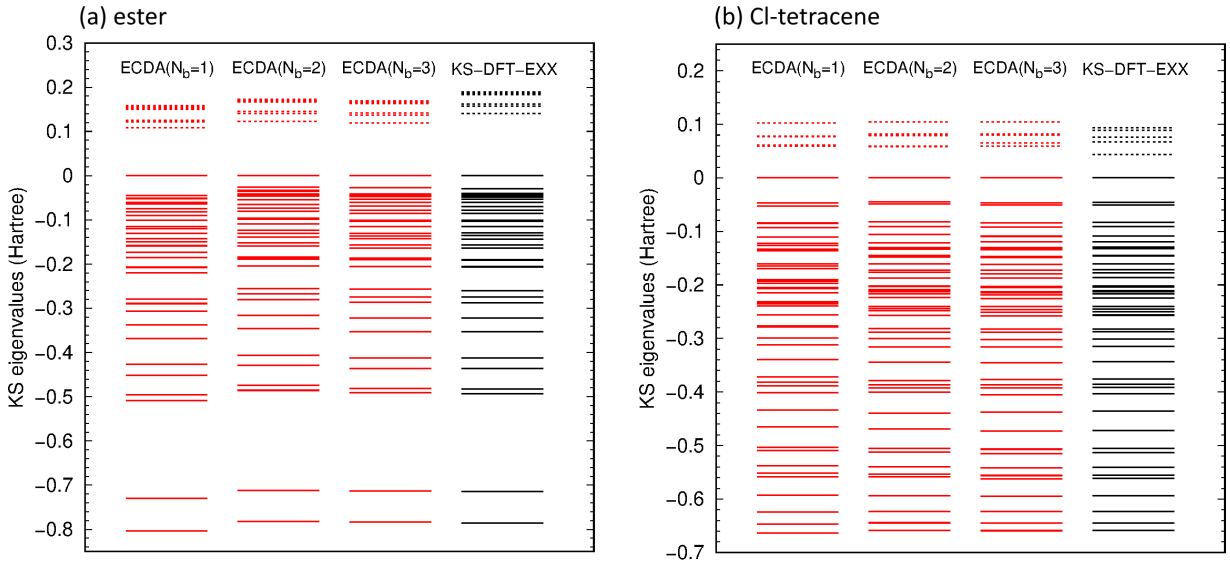

Figure 6: KS orbital energies of (a) ester and (b) Cl-tetracene from self-consistent ECDA-envOF(TF) calculations with different N_b values and self-consistent KS-DFT-EXX calculations (benchmark). Occupied and unoccupied orbitals are indicated by solid and dashed lines, respectively. The orbital energies of highest occupied orbitals are set to zero for easy comparison.

4.2 Performance of ECDA-envOF(TF) on carbon chains

Three polymers (polyyne, polyacetylene, and polyethylene) were recently used to investigate the performance of the periodic density embedding theory[92] (a variant of the density matrix embedding theory[20] by adjusting a bath's chemical potential). And polyyne was also used to examine the performance of the periodic density matrix embedding theory.[93] Here, we examine the performance of ECDA on similar systems. Since we have not implemented ECDA for the periodic boundary condition, we cannot simulate these polymers here. Instead, we perform ECDA calculations on three molecules (a) $C_{10}H_2$, (b) $C_{12}H_{14}$, and (c) $C_{12}H_{26}$, to mimic these polymers. Structures of these molecules are shown in Fig. 7. $C_{10}H_2$ has an alternating C≡C-C structure for mimicking polyyne. $C_{12}H_{14}$ has an alternating C=C-

C structure for mimicking polyacetylene. $C_{12}H_{26}$ mimics polyethylene. Details of these structures are given in the "Numerical Details" section. In what follows, we examine the performance of ECDA-envOF(TF) for patching EXX energies in these molecules.

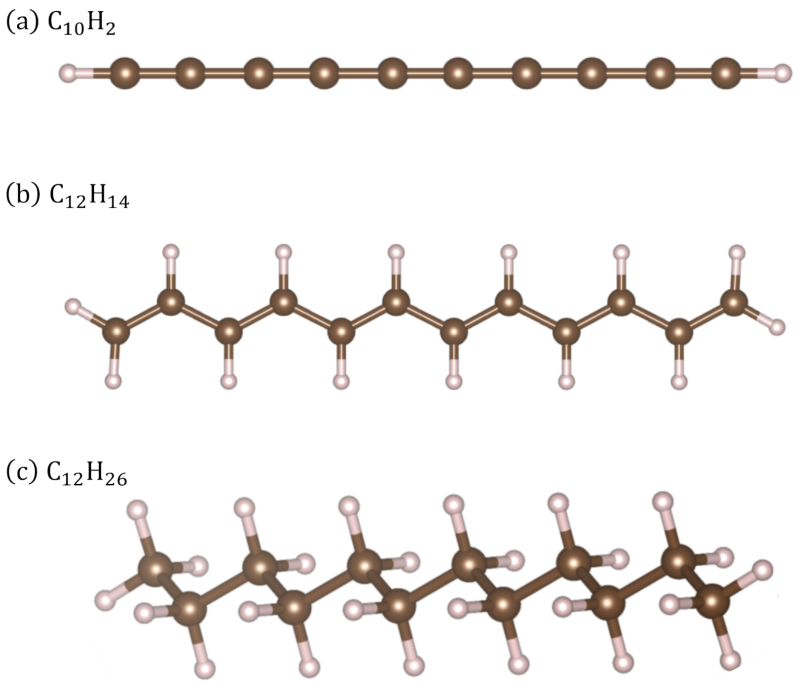

Figure 7: Structures of (a) $C_{10}H_2$, (b) $C_{12}H_{14}$, and (c) $C_{12}H_{26}$. Carbon atoms are brown and hydrogen atoms are grey.

All carbon chains are uniformly stretched/compressed by a scaling factor α. Only carbon-carbon bonds are scaled by α, and other geometry parameters are kept fixed, except $C_{12}H_{26}$ for which the six hydrogen atoms at its two ends are optimized for different α values. Fig. 8 shows the total energies versus the scaling factor α. ECDA results converge to KS-DFT-EXX results as N_b increases. In the lower subplots, we plot the energy error per atom. For all molecules, the errors are smaller than 5 mHa by including atoms up to the third nearest neighbors (i.e., $N_b = 3$) for defining the clusters.

Fig. 8 also shows that all ECDA energy curves are smooth. Smooth energy curves are important for structure-related calculations, e.g., structure optimization and phonon calculations. The smoothness is largely due to the use of density partitioning for defining clusters, which makes the clusters' electronic structures to change smoothly as the molecules are

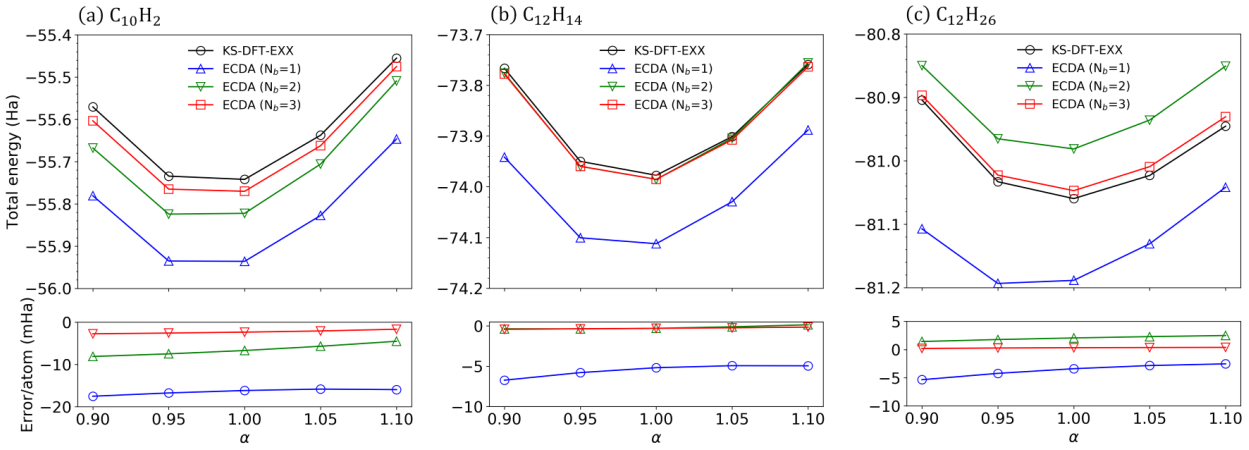

Figure 8: Total energies versus scaling factor α for $C_{10}H_2$, $C_{12}H_{14}$, and $C_{12}H_{26}$ from self-consistent KS-DFT-EXX and self-consistent ECDA-envOF(TF) calculations. Errors per atom are shown in lower subplots.

stretched/compressed. This is different from the local correlation methods based on localized molecular orbitals. In these methods, localized molecular orbitals need to be carefully selected to make sure that clusters' electronic structures change smoothly as molecular structure changes. This is challenging, if some localized orbitals span both the cluster and the environment. Density partitioning does not have such problem, because clusters are defined by directly cutting the bonds at cluster-environment boundary. However, this causes one problem: The dangling bonds at the cluster-environment interfaces can affect the electronic structures inside the clusters. This is expected to be the reason for the zigzag convergence observed for $C_{12}H_{26}$: The energy curves of $N_b = 1$ and $N_b = 3$ are lower than the benchmark, while the energy curve of $N_b = 2$ is higher than the benchmark. Nevertheless, for a given N_b, ECDA produces smooth energy curves that follow well with the benchmarks. Such good agreement should be largely due to the fact that density embedding suppresses the effect from the dangling bonds by enforcing the cluster and the system's electron densities to match inside the cluster.

In Figure 9, we examine the KS eigenvalues from KS-DFT-EXX and ECDA-envOF(TF) calculations. Their agreement on the occupied orbitals becomes better as N_b increases; however, ECDA's predictions for the gaps between the highest-occupied molecular orbitals

(HOMOs) and the lowest occupied molecular orbitals (LUMOs) (Table 3) are not improved by increasing N_b. It is not clear why ECDA's gaps decrease slightly as N_b increases from 1 to 3. By comparing Figure 8 and Table 3, we find no much correlation between the convergence of the total energies and the convergence of the HOMO-LUMO gaps. ECDA gives the largest error for $C_{10}H_2$'s energies but gives the best predictions for $C_{10}H_2$'s HOMO-LUMO gaps.

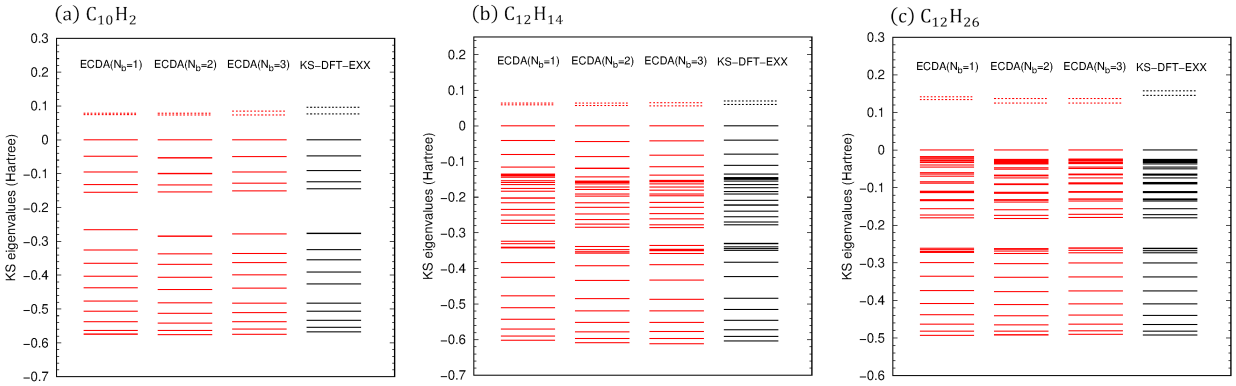

Figure 9: KS orbital energies from self-consistent ECDA-envOF(TF) and self-consistent KS-DFT-EXX calculations (benchmark) for $\alpha = 1$. Occupied and unoccupied orbitals are indicated by solid and dashed lines, respectively. The highest occupied orbitals are shifted to zero for easy comparison.

Table 3: HOMO-LUMO gaps (in eV) from self-consistent KS-DFT-EXX and self-consistent ECDA-envOF(TF) calculations (with different N_b).

	$C_{10}H_2$	$C_{12}H_{14}$	$C_{12}H_{26}$
KS-DFT-EXX	2.09	1.63	3.95
ECDA (N_b=1)	2.04	1.61	3.66
ECDA (N_b=2)	1.99	1.56	3.40
ECDA (N_b=3)	1.99	1.54	3.40

4.3 Performance of ECDA-envOF(TF) on the Na and MgO nanorods

In the previous sections, we have investigated the performance of ECDA-envOF(TF) on several covalent systems. In what follows, we investigate its performance on one metallic (a Na nanorod) and one ionic system (a MgO nanorod). Details about their structures and calculations are given in the "Numerical details" section. For both nanorods, we examine

the energy versus a uniform scaling of the rods' lengths. To obtain smooth energy curves, for different N_b values the clusters are defined based on the unscaled structures. For each atom, its nearest neighbors are defined according to the bonds shown in Figure 10.

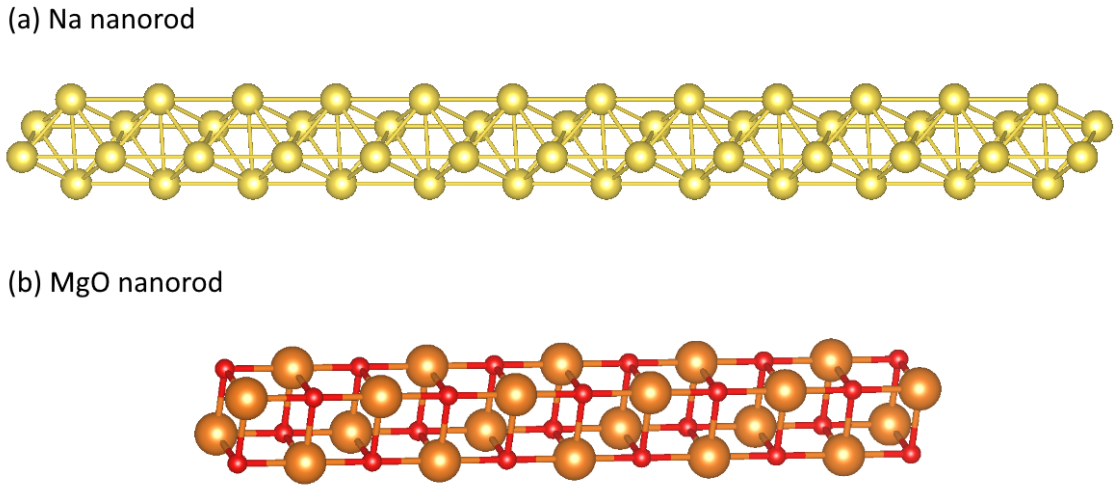

Figure 10: The structures of (a) Na and (b) MgO nanorods. In subplot (b), oxygen atoms are red and Mg atoms are brown.

Figure 11 gives the total energy versus the scaling for the Na nanorod. The ECDA curve with $N_b = 1$ deviates from the KS-DFT-EXX curve for $\alpha > 1$, due to the fact that the density matrix decays slowly in metallic systems and therefore clusters defined by $N_b = 1$ cannot capture the long-range exchange. The ECDA energy curve is much improved by using larger clusters (i.e., $N_b = 2$ and 3). Figure 12 shows the energy versus the scaling for the MgO nanorod. Even with $N_b = 1$, ECDA's energy curve agrees well with the KS-DFT-EXX curve, due to the fact that the density matrix decays fast in this ionic system. In addition, the error per atom is much less than the Na nanorod. One puzzle is that the errors do not decrease much for large N_b. $N_b = 3$ is expected to produce smaller errors than $N_b = 1$; however they give similar errors. To check whether this unexpected observation is due to the finite η used in the Zhao-Parr method, we increased η to 2×10^6 for the $\alpha = 1.0$ case and found that the changes of the total energies are less than 1 mHa. Therefore, this unexpected observation seems not to be due to a finite η. The reason for this unexpected observation is still unclear at this point and should be investigated in the future work.

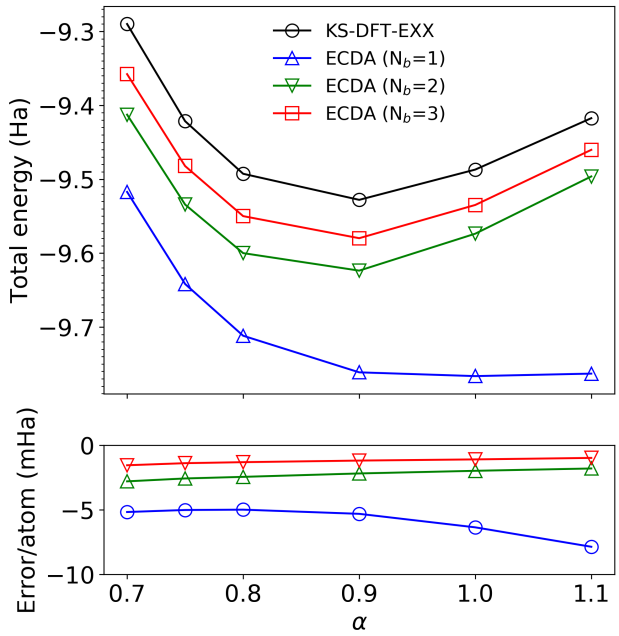

Figure 11: Total energy versus a uniform scaling of the Na nanorod from self-consistent KS-DFT-EXX and self-consistent ECDA-envOF(TF) calculations. The lower subplot gives the total energy error per atom.

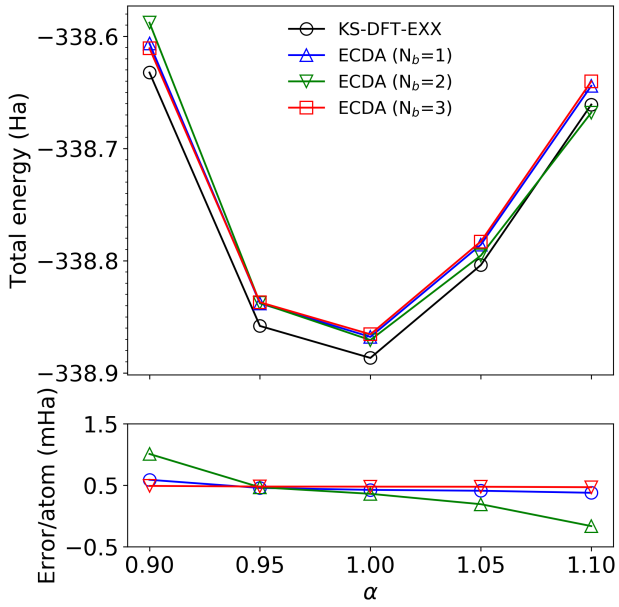

Figure 12: Total energy versus a uniform scaling of the MgO nanorod from self-consistent KS-DFT-EXX and self-consistent ECDA-envOF(TF) calculations. The low subplot gives the total energy error per atom.

5 Computational aspect of ECDA

Compared to a conventional KS-DFT calculation on the full system, ECDA saves the cost by calculating the system's XC energy in an atom-by-atom manner. Its overhead is mainly from two tasks: (1) the density partitioning using the Zhao-Parr method and (2) solving $z(\mathbf{r})$ with Eq. 56. The overhead cost can be much reduced by treating the environments with OF-DFT. Taking the MgO nanorod for example, we briefly show the reduction of the overhead cost. Both ECDA-envOF(TF) and ECDA-envKS calculations are performed with $N_b = 3$. For ECDA-envKS calculations, we assign one CPU for each cluster and one CPU for each environment. For ECDA-envOF calculations, each cluster together with its environment is solved by one CPU. This shows another benefit from treating the environments with OF-DFT: The number of CPUs can be reduced by half. With ECDA-envOF(TF), the average cost of each iteration of the Zhao-Parr method is nearly halved: 38 seconds for ECDA-envOF(TF) and 76 seconds for ECDA-envKS. The average cost of each iteration for solving $z(\mathbf{r})$ is reduced by 33%: 9 seconds for ECDA-envOF(TF) and 14 seconds for ECDA-envKS. The cost reduction should be more significant for large systems.

We note that our current implementation of ECDA is inefficient: a system and its clusters are put in the same unit cell. This makes the costs of these cluster calculations in tasks (1) and (2) scale with the system's size. In the future, clusters will be put in the super cells whose sizes are determined by the clusters. This will further reduce the overhead cost.

For large systems, ECDA-envOF's computational cost will be dominated by the following tasks: (a) solving the system's KS equation, (b) solving the system's OEP equation (Eq. 34), and (c) calculating p_1 in Eq. 54. The cost of task (a) is determined by the implementation of KS-DFT and can be reduced by combining ECDA with linear-scaling KS-DFT methods.[94,95] Tasks (b) and (c) are costly, since they depend on solving the system's Sternheimer equation. In addition, task (b) is about N_{oep} times more expensive than task (c), where N_{oep} is the number of iterations for solving the system's OEP equation. In the future work, we will try to completely avoid task (b) by directly minimizing the system's energy against its KS

potential (v_s) as suggested by Yang and Wu.[96]

6 Conclusions

By treating environments with OF-DFT, in this work we have removed two computational bottlenecks in ECDA calculations: (a) partitioning the system's electron density among clusters and environments and (b) calculating environments' linear responses for building the system's XC potential. With two examples (ester and Cl-tetracene), we showed that ECDA-envOF and ECDA-envKS gave very similar results even with small clusters. Therefore, ECDA-envOF can be used in future ECDA calculations. Two KEDFs (TFm and TFm+1/9vWm) were employed for treating environments. Their performances were similar. Since the cost of OF-DFT calculations with TFm KEDF is much less, ECDA-envOF(TF) should be used in future calculations.

Another focus of this work is to investigate ECDA-envOF(TF)'s performance on different types of systems: covalent, metallic, and ionic. For covalent systems, we employ ECDA-envOF(TF) to study three hydrocarbons that have different types of carbon-carbon bonds. The energy curves for stretching/compressing these molecules followed the benchmarks well even for clusters that only contain the nearest neighbors. For metallic and ionic systems, we examined the Na and MgO nanorods. Due to the slow decay of the density matrix in metallic systems, it is found that clusters need include atoms up to the second nearest neighbors for the Na nanorod. For the MgO nanorod, even with $N_b = 1$, ECDA-envOF(TF) results agreed well with the benchmark, due to the fast decay of the density matrix in ionic systems. These examples demonstrate that ECDA's performance depends on how rapidly electron correlation decays. It was also observed that the energy curves for stretching/compressing these systems were smooth, which suggests that ECDA-envOF(TF) is applicable to structure-related tasks, such as geometry optimization and phonon calculations. Forces are needed for structure-related tasks and can be derived for ECDA-envOF(TF) following the similar way as in our

recent work.[51]

In summary, by removing the computational bottlenecks related to environment calculations and showing the good performance of ECDA-envOF(TF) in systems with different types of bonds, we expect ECDA-envOF(TF) to become an efficient and nearly black-box local correlation method for scaling up high-level KS-DFT calculations in large heterogeneous materials.

Acknowledgement

This work is supported by the National Science Foundation CAREER award, with the number: #1752769. Some calculations were performed using the Extreme Science and Engineering Discovery Environment (XSEDE)[97] supported by the National Science Foundation Grant No. ACI-1548562, with the allocation number TG-CHE180077.

A Linear response for a system treated by OF-DFT with TFm KEDF

For the case that environments are treated by TFm KEDF, their total energies are $E_{\mathrm{OF}} = T_{\mathrm{TFm}}[\rho] + \int \rho(\mathbf{r}) v(\mathbf{r}) dr^3$, where v is the external potential. Note that Hartree and XC energies are not considered, since environments are modeled as non-interacting electron systems. We then have $v_{\mathrm{TFm}}(\mathbf{r}) + v(\mathbf{r}) = \mu$, where $v_{\mathrm{TFm}}(\mathbf{r}) = \delta T_{\mathrm{TFm}} / \delta \rho(\mathbf{r})$ and μ is the chemical potential. Linearizing the equation for a given Δv, the perturbed electron density is

$$\Delta\rho(\mathbf{r}) = (\Delta\mu - \Delta v(\mathbf{r}))/K_{\mathrm{TFm}}(\mathbf{r}), \tag{57}$$

where $K_{\mathrm{TFm}}(\mathbf{r},\mathbf{r}') = \delta^2 T_{\mathrm{TFm}}/\delta\rho(\mathbf{r})\rho(\mathbf{r}')$ is TFm's kernel. $\Delta\mu$ is calculated based on the conservation of electron density $\int \Delta\rho(\mathbf{r})dr^3 = 0$:

$$\Delta\mu = \frac{\int K^{-1}_{\mathrm{TFm}}(\mathbf{r},\mathbf{r})\Delta v(\mathbf{r})d^3r}{\int K^{-1}_{\mathrm{TFm}}(\mathbf{r},\mathbf{r})d^3r}. \tag{58}$$

B Linear response for systems treated by OF-DFT using TFm+λvWm KEDF

For the case that an environment is treated by TFm+λvWm KEDF, its total energy is

$$E_{\mathrm{OF}} = T_{\mathrm{TFm}}[\rho] + \lambda T_{\mathrm{vWm}}[\rho] + \int \rho(\mathbf{r})v(\mathbf{r})d^3r. \tag{59}$$

Define the Lagrangian

$$L_{\mathrm{OF}} = E_{\mathrm{OF}} - \mu\left(\int \phi(\mathbf{r})^2 d^3r - N\right), \tag{60}$$

where $\phi(\mathbf{r}) = \sqrt{\rho(\mathbf{r})}$. The last term is for conserving the electron number N. μ is the Lagrangian multiplier. Based on $\delta L_{\mathrm{OF}}/\delta\phi(\mathbf{r}) = 0$ and replacing ϕ with ϕ_{m}, we obtain the equation for ϕ_{m}

$$H_{\mathrm{OF}}\left|\phi_{\mathrm{m}}\right\rangle = \mu\left|\phi_{\mathrm{m}}\right\rangle, \tag{61}$$

with $H_{\mathrm{OF}} = -\frac{1}{2}\nabla^2 + v_{\mathrm{scf}}$ and $v_{\mathrm{scf}}(\mathbf{r}) = (v_{\mathrm{TFm}}(\mathbf{r}) + v(\mathbf{r}))/\lambda$. Given a perturbing potential Δv_{scf}, the perturbation $\Delta\phi_{\mathrm{m}}$ can be calculated using the Sternheimer equation

$$\left[H_{\mathrm{OF}} - \mu + P_v\right]\left|\Delta\phi_{\mathrm{m}}\right\rangle = -P_c M\left|\Delta v_{\mathrm{scf}}\right\rangle, \tag{62}$$

where $P_v = \left|\phi_{\mathrm{m}}\right\rangle\left\langle\phi_{\mathrm{m}}\right|$ is the projector to the occupied space and $P_c = 1 - P_v$. M is a matrix whose diagonal elements are ϕ_{m}, that is, $M(\mathbf{r},\mathbf{r}') = \delta(\mathbf{r}-\mathbf{r}')\phi_{\mathrm{m}}(\mathbf{r})$. Since Δv_{scf} depends on $\Delta\phi_{\mathrm{m}}$, we have to solve above equation self-consistently as in conventional density functional perturbation theory. To avoid solving Eq. 62 self-consistently, we can write Δv_{scf} in terms

of Δv and $\Delta\phi_{\mathrm{m}}$

$$|\Delta v_{\mathrm{scf}}\rangle = |\Delta v\rangle + \frac{2}{\lambda} K_{\mathrm{TFm}} M \, |\Delta\phi_{\mathrm{m}}\rangle \, . \tag{63}$$

After inserting $|\Delta v_{\mathrm{scf}}\rangle$ into Eq. 62, we obtain the equation for $|\Delta\phi_{\mathrm{m}}\rangle$

$$\left[H_{\mathrm{OF}} - \mu + P_v + \frac{2}{\lambda} P_c M K_{\mathrm{TFm}} M \right] |\Delta\phi_{\mathrm{m}}\rangle = -P_c M \, |\Delta v\rangle \, . \tag{64}$$

The above linear system cannot be solved using the conjugate gradient method, since the operator $P_c M K_{\mathrm{TFm}} M$ on left-hand side is not symmetric. To overcome this issue, we can replace it with $P_c M K_{\mathrm{TFm}} M P_c$, due to the fact that $|\Delta\phi_{\mathrm{m}}\rangle$ is orthogonal to ϕ_{m}. Since $P_c M K_{\mathrm{TFm}} M P_c$ is positive-definite and symmetric, Eq. 64 can be solved by the conjugate gradient method. After obtaining $\Delta\phi_{\mathrm{m}}$, the perturbed electron density is calculated by $\Delta\rho(\mathbf{r}) = 2\phi_{\mathrm{m}}(\mathbf{r})\Delta\phi_{\mathrm{m}}(\mathbf{r})$.

C The calculation of $\delta\rho(\mathbf{r})/\delta N$ for systems treated by OF-DFT using TFm+λvWm KEDF

Consider a system with its total energy defined by Eq. 59. Normalize ϕ_{m} as $\phi'(\mathbf{r}) = \phi_{\mathrm{m}}(\mathbf{r})/\sqrt{N + \Omega\rho_0}$, where Ω is the volume of the simulation cell, and we have $\int \phi'(\mathbf{r})^2 d^3r = 1$. ϕ' is related to ρ as

$$\rho(\mathbf{r}) + \rho_0 = (N + \Omega\rho_0)[\phi'(\mathbf{r})]^2. \tag{65}$$

Note that ϕ' is also the solution to Eq. 61, and therefore the Sternheimer equation for solving $\Delta\phi'$ (due to Δv_{scf}) is similar to Eq. 62 and is

$$[H_{\mathrm{OF}} - \mu + P_v] \, |\Delta\phi'\rangle = -P_c M' \, |\Delta v_{\mathrm{scf}}\rangle \, , \tag{66}$$

where $P_v = |\phi'\rangle \langle\phi'|$ and $P_c = 1 - P_v$. M' is a diagonal matrix with the diagonal elements equal to ϕ' (i.e., $M'(\mathbf{r}, \mathbf{r}) = \phi'(\mathbf{r})$). Since Δv_{scf} depends on $\Delta\phi'$, Eq. 66 has to solved self-

consistently. To avoid solving Eq. 66 self-consistently, we derive the expression for Δv_{scf}. Based on Eq. 65, a change of electron number (δN) causes a change in $\rho(\mathbf{r})$ as

$$\delta\rho(\mathbf{r}) = \phi'(\mathbf{r})^2\delta N + 2(N+\Omega\rho_0)\phi'(\mathbf{r})\delta\phi'(\mathbf{r}). \tag{67}$$

$\delta\rho$ then causes a change in v_{scf} as

$$\begin{aligned}\delta v_{\mathrm{scf}}(\mathbf{r}) &= \int \frac{\delta v_{\mathrm{scf}}(\mathbf{r})}{\delta\rho(\mathbf{r}')}\delta\rho(\mathbf{r}')d^3r' \\ &= \frac{\delta N}{\lambda}\int K_{\mathrm{TFm}}(\mathbf{r},\mathbf{r}')\phi'(\mathbf{r}')^2 d^3r' + \frac{2(N+\Omega\rho_0)}{\lambda}\int K_{\mathrm{TFm}}(\mathbf{r},\mathbf{r}')\phi'(\mathbf{r}')\delta\phi'(\mathbf{r}')d^3r'\end{aligned} \tag{68}$$

Inserting Eq. 68 into Eq. 66, we obtain the equation for $\Delta\phi'$

$$\left[H_{\mathrm{OF}} - \mu + P_v + \frac{2(N+\Omega\rho_0)}{\lambda}P_cM'K_{\mathrm{TFm}}M'\right]\Delta\phi'(\mathbf{r}) = -\frac{1}{\lambda}P_cM'K_{\mathrm{TFm}}\phi'(\mathbf{r})^3. \tag{69}$$

Again, we can make above linear system to be symmetric by replacing $P_cM'K_{\mathrm{TFm}}M'$ with $P_cM'K_{\mathrm{TFm}}M'P_c$, due to the fact that $\Delta\phi'$ is orthogonal to ϕ'. The new linear system can then be solved using the conjugate gradient method. Finally $\delta\rho/\delta N$ is given by

$$\frac{\delta\rho(\mathbf{r})}{\delta N} = \phi'(\mathbf{r})^2 + 2(N+\Omega\rho_0)\phi'(\mathbf{r})\Delta\phi'(\mathbf{r}). \tag{70}$$

References

(1) Saebø, S.; Pulay, P. Local treatment of electron correlation. *Annual Review of Physical Chemistry* **1993**, *44*, 213–236.

(2) Kohn, W. Density functional and density matrix method scaling linearly with the number of atoms. *Physical Review Letters* **1996**, *76*, 3168.

(3) Prodan, E.; Kohn, W. Nearsightedness of electronic matter. *Proceedings of the National*

Academy of Sciences of the United States of America **2005**, *102*, 11635–11638.

(4) Stoll, H. Correlation energy of diamond. *Phys. Rev. B* **1992**, *46*, 6700–6704.

(5) Stoll, H. On the correlation energy of graphite. *The Journal of Chemical Physics* **1992**, *97*, 8449–8454.

(6) Pulay, P. Localizability of dynamic electron correlation. *Chemical physics letters* **1983**, *100*, 151–154.

(7) Saebø, S.; Pulay, P. Local configuration interaction: An efficient approach for larger molecules. *Chemical physics letters* **1985**, *113*, 13–18.

(8) Kirtman, B.; Dykstra, C. E. Local space approximation for configuration interaction and coupled cluster wave functions. *The Journal of chemical physics* **1986**, *85*, 2791–2796.

(9) Hampel, C.; Werner, H.-J. Local treatment of electron correlation in coupled cluster theory. *The Journal of chemical physics* **1996**, *104*, 6286–6297.

(10) Scuseria, G. E.; Ayala, P. Y. Linear scaling coupled cluster and perturbation theories in the atomic orbital basis. *The Journal of chemical physics* **1999**, *111*, 8330–8343.

(11) Schütz, M.; Werner, H.-J. Local perturbative triples correction (T) with linear cost scaling. *Chemical Physics Letters* **2000**, *318*, 370–378.

(12) Constans, P.; Ayala, P. Y.; Scuseria, G. E. Scaling reduction of the perturbative triples correction (T) to coupled cluster theory via Laplace transform formalism. *The Journal of Chemical Physics* **2000**, *113*, 10451–10458.

(13) Maslen, P.; Lee, M.; Head-Gordon, M. An accurate local model for triple substitutions in fourth order Møller-Plesset theory and in perturbative corrections to singles and doubles coupled cluster methods. *Chemical Physics Letters* **2000**, *319*, 205–212.

(14) Pulay, P.; Saebø, S. Orbital-invariant formulation and second-order gradient evaluation in Moller-Plesset perturbation theory. *Theoretica Chimica Acta* **1986**, *69*, 357–368.

(15) Saebø, S.; Pulay, P. Fourth-order Møller-Plesset perturbation theory in the local correlation treatment. I. Method. *The Journal of chemical physics* **1987**, *86*, 914–922.

(16) Murphy, R. B.; Beachy, M. D.; Friesner, R. A.; Ringnalda, M. N. Pseudospectral localized Møller-Plesset methods: Theory and calculation of conformational energies. *The Journal of chemical physics* **1995**, *103*, 1481–1490.

(17) Maslen, P. E.; Head-Gordon, M. Noniterative local second order Mo/ller–Plesset theory: Convergence with local correlation space. *The Journal of Chemical Physics* **1998**, *109*, 7093–7099.

(18) Hetzer, G.; Pulay, P.; Werner, H.-J. Multipole approximation of distant pair energies in local MP2 calculations. *Chemical Physics Letters* **1998**, *290*, 143–149.

(19) Novák, P.; Kuneš, J.; Chaput, L.; Pickett, W. Exact exchange for correlated electrons. *physica status solidi (b)* **2006**, *243*, 563–572.

(20) Knizia, G.; Chan, G. K.-L. Density matrix embedding: A simple alternative to dynamical mean-field theory. *Physical Review Letters* **2012**, *109*, 186404.

(21) Manby, F. R.; Stella, M.; Goodpaster, J. D.; Miller III, T. F. A simple, exact density-functional-theory embedding scheme. *Journal of chemical theory and computation* **2012**, *8*, 2564–2568.

(22) Fornace, M. E.; Lee, J.; Miyamoto, K.; Manby, F. R.; Miller III, T. F. Embedded Mean-Field Theory. *Journal of chemical theory and computation* **2015**, *11*, 568–580.

(23) Pernal, K. Reduced density matrix embedding: General formalism and inter-domain correlation functional. *Physical Chemistry Chemical Physics* **2016**, *18*, 21111–21121.

(24) Bulik, I. W.; Scuseria, G. E.; Dukelsky, J. Density matrix embedding from broken symmetry lattice mean fields. *Physical Review B* **2014**, *89*, 035140.

(25) Welborn, M.; Tsuchimochi, T.; Voorhis, T. V. Bootstrap embedding: An internally consistent fragment-based method. *The Journal of Chemical Physics* **2016**, *145*, 074102.

(26) Yu, K.; Carter, E. A. Extending density functional embedding theory for covalently bonded systems. *Proceedings of the National Academy of Sciences* **2017**, *114*, E10861–E10870.

(27) Mordovina, U.; Reinhard, T. E.; Theophilou, I.; Appel, H.; Rubio, A. Self-Consistent Density-Functional Embedding: A Novel Approach for Density-Functional Approximations. *Journal of Chemical Theory and Computation* **2019**, *15*, 5209–5220.

(28) Metzner, W.; Vollhardt, D. Correlated lattice fermions in d=∞ dimensions. *Physical Review Letters* **1989**, *62*, 324.

(29) Georges, A.; Krauth, W. Numerical solution of thed=∞ Hubbard model: Evidence for a Mott transition. *Physical Review Letters* **1992**, *69*, 1240–1243.

(30) Georges, A.; Kotliar, G.; Krauth, W.; Rozenberg, M. J. Dynamical mean-field theory of strongly correlated fermion systems and the limit of infinite dimensions. *Reviews of Modern Physics* **1996**, *68*, 13.

(31) Chibani, W.; Ren, X.; Scheffler, M.; Rinke, P. Self-consistent Green's function embedding for advanced electronic structure methods based on a dynamical mean-field concept. *Physical Review B* **2016**, *93*, 165106.

(32) Lan, T. N.; Kananenka, A. A.; Zgid, D. Communication: Towards ab initio self-energy embedding theory in quantum chemistry. *The Journal of Chemical Physics* **2015**, *143*, 241102.

(33) Senatore, G.; Subbaswamy, K. R. Density dependence of the dielectric constant of rare-gas crystals. *Physical Review B* **1986**, *34*, 5754.

(34) Cortona, P. Self-consistently determined properties of solids without band-structure calculations. *Physical Review B* **1991**, *44*, 8454.

(35) Wesolowski, T. A.; Warshel, A. Frozen density functional approach for ab initio calculations of solvated molecules. *The Journal of Physical Chemistry* **1993**, *97*, 8050–8053.

(36) Govind, N.; Wang, Y.; Da Silva, A.; Carter, E. A. Accurate ab initio energetics of extended systems via explicit correlation embedded in a density functional environment. *Chemical physics letters* **1998**, *295*, 129–134.

(37) Kohn, W.; Mattsson, A. E. Edge electron gas. *Physical Review Letters* **1998**, *81*, 3487.

(38) Cohen, M. H.; Wasserman, A. On hardness and electronegativity equalization in chemical reactivity theory. *Journal of statistical physics* **2006**, *125*, 1121–1139.

(39) Neugebauer, J.; Louwerse, M. J.; Baerends, E. J.; Wesolowski, T. A. The merits of the frozen-density embedding scheme to model solvatochromic shifts. *The Journal of Chemical Physics* **2005**, *122*, 094115.

(40) Jacob, C. R.; Visscher, L. Calculation of nuclear magnetic resonance shieldings using frozen-density embedding. *The Journal of chemical physics* **2006**, *125*, 194104.

(41) Roncero, O.; de Lara-Castells, M. P.; Villarreal, P.; Flores, F.; Ortega, J.; Paniagua, M.; Aguado, A. An inversion technique for the calculation of embedding potentials. *The Journal of Chemical Physics* **2008**, *129*, 184104.

(42) Goodpaster, J. D.; Ananth, N.; Manby, F. R.; Miller III, T. F. Exact nonadditive kinetic potentials for embedded density functional theory. *The Journal of chemical physics* **2010**, *133*, 084103.

(43) Elliott, P.; Burke, K.; Cohen, M. H.; Wasserman, A. Partition density-functional theory. *Physical Review A* **2010**, *82*, 024501.

(44) Huang, C.; Pavone, M.; Carter, E. A. Quantum mechanical embedding theory based on a unique embedding potential. *The Journal of chemical physics* **2011**, *134*, 154110.

(45) Laricchia, S.; Fabiano, E.; Della Sala, F. Frozen density embedding with hybrid functionals. *The Journal of chemical physics* **2010**, *133*, 164111.

(46) Fux, S.; Jacob, C. R.; Neugebauer, J.; Visscher, L.; Reiher, M. Accurate frozen-density embedding potentials as a first step towards a subsystem description of covalent bonds. *The Journal of chemical physics* **2010**, *132*, 164101.

(47) Pavanello, M.; Neugebauer, J. Modelling charge transfer reactions with the frozen density embedding formalism. *The Journal of chemical physics* **2011**, *135*, 234103.

(48) Zhu, T.; de Silva, P.; van Aggelen, H.; Van Voorhis, T. Many-electron expansion: A density functional hierarchy for strongly correlated systems. *Physical Review B* **2016**, *93*, 201108.

(49) Huang, C. Extending the density functional embedding theory to finite temperature and an efficient iterative method for solving for embedding potentials. *The Journal of chemical physics* **2016**, *144*, 124106.

(50) Huang, C. Patching the Exchange-Correlation Potential in Density Functional Theory. *Journal of chemical theory and computation* **2016**, *12*, 2224–2233.

(51) Huang, C. Analytical energy gradient for the embedded cluster density approximation. *The Journal of Chemical Physics* **2019**, *151*, 134101.

(52) Hohenberg, P.; Kohn, W. Inhomogeneous electron gas. *Physical Review* **1964**, *136*, B864.

(53) Kohn, W.; Sham, L. J. Self-consistent equations including exchange and correlation effects. *Physical Review* **1965**, *140*, A1133.

(54) Huang, C. Embedded Cluster Density Approximation for Exchange–Correlation Energy: A Natural Extension of the Local Density Approximation. *Journal of Chemical Theory and Computation* **2018**, *14*, 6211–6225.

(55) Smargiassi, E.; Madden, P. A. Orbital-free kinetic-energy functionals for first-principles molecular dynamics. *Physical Review B* **1994**, *49*, 5220–5226.

(56) Govind, N.; Mozos, J.-L.; Guo, H. Equilibrium structure and bonding of small silicon clusters studied using an orbital-free kinetic-energy functional. *Physical Review B* **1995**, *51*, 7101–7103.

(57) Nehete, D.; Shah, V.; Kanhere, D. G. Abinitiomolecular dynamics using density-based energy functionals: Application to ground-state geometries of some small clusters. *Physical Review B* **1996**, *53*, 2126–2131.

(58) Wang, Y.; Carter, E. In *Theoretical Methods in CondensedPhase Chemistry*; Schwartz, S., Ed.; Kluwer Academic Publishers, 2002; Chapter Orbital-free kinetic-energy density functional theory, p 117.

(59) Huang, C. Wavelength-decomposition-based embedded cluster density approximation for systems with nonlocal electron correlation. *International Journal of Quantum Chemistry* **2020**,

(60) Sharp, R.; Horton, G. A variational approach to the unipotential many-electron problem. *Physical Review* **1953**, *90*, 317.

(61) Talman, J. D.; Shadwick, W. F. Optimized effective atomic central potential. *Physical Review A* **1976**, *14*, 36.

(62) Sahni, V.; Gruenebaum, J.; Perdew, J. Study of the density-gradient expansion for the exchange energy. *Physical Review B* **1982**, *26*, 4371.

(63) Kümmel, S.; Kronik, L. Orbital-dependent density functionals: Theory and applications. *Reviews of Modern Physics* **2008**, *80*, 3.

(64) Harl, J.; Schimka, L.; Kresse, G. Assessing the quality of the random phase approximation for lattice constants and atomization energies of solids. *Physical Review B* **2010**, *81*, 115126.

(65) Harris, J.; Jones, R. O. The surface energy of a bounded electron gas. *J. Phys. F: Met. Phys.* **1974**,

(66) Langreth, D. C.; Perdew, J. P. The exchange-correlation energy of a metallic surface. *Solid State Communications* **1975**, *17*, 1425–1429.

(67) Gunnarsson, O.; Lundqvist, B. I. Exchange and correlation in atoms, molecules, and solids by the spin-density-functional formalism. *Phys. Rev. B* **1976**,

(68) Langreth, D. C.; Perdew, J. P. Exchange-correlation energy of a metallic surface wavevector analysis. *Physical Review B* **1977**, *15*, 2884.

(69) Yan, Z.; Perdew, J. P.; Kurth, S. Density functional for short-range correlation: Accuracy of the random-phase approximation for isoelectronic energy changes. *Physical Review B* **2000**, *61*, 16430.

(70) Perdew, J. P.; Wang, Y. Accurate and simple analytic representation of the electron-gas correlation energy. *Physical Review B* **1992**, *45*, 13244–13249.

(71) Thomas, L. The calculation of atomic fields. Mathematical Proceedings of the Cambridge Philosophical Society. 1927; pp 542–548.

(72) Fermi, E. *Rend. Acad. Maz. Lancei* **1927**, *6*, 602.

(73) von Weizsäcker, C. *Z. Phys.* **1935**, *96*, 431.

(74) Zhao, Q.; Parr, R. G. Quantities Ts[n] and Tc[n] in density-functional theory. *Physical Review A* **1992**, *46*, 2337.

(75) Zhao, Q.; Morrison, R. C.; Parr, R. G. From electron densities to Kohn-Sham kinetic energies, orbital energies, exchange-correlation potentials, and exchange-correlation energies. *Physical Review A* **1994**, *50*, 2138.

(76) Pulay, P. Convergence acceleration of iterative sequences. the case of scf iteration. *Chem. Phys. Lett.* **1980**, *73*, 393–398.

(77) Baroni, S.; Giannozzi, P.; Testa, A. Green's-function approach to linear response in solids. *Physical Review Letters* **1987**, *58*, 1861–1864.

(78) de Gironcoli, S. Lattice dynamics of metals from density-functional perturbation theory. *Physical Review B* **1995**, *51*, 6773–6776.

(79) Baroni, S.; de Gironcoli, S.; Corso, A. D.; Giannozzi, P. Phonons and related crystal properties from density-functional perturbation theory. *Reviews of Modern Physics* **2001**, *73*, 515–562.

(80) Gonze, X.; Amadon, B.; Anglade, P.-M.; Beuken, J.-M.; Bottin, F.; Boulanger, P.; Bruneval, F.; Caliste, D.; Caracas, R.; Côté, M., et al. ABINIT: First-principles approach to material and nanosystem properties. *Computer Physics Communications* **2009**, *180*, 2582–2615.

(81) Genovese, L.; Deutsch, T.; Neelov, A.; Goedecker, S.; Beylkin, G. Efficient solution of Poisson's equation with free boundary conditions. *The Journal of Chemical Physics* **2006**, *125*, 074105.

(82) Momma, K.; Izumi, F. VESTA 3for three-dimensional visualization of crystal, volumetric and morphology data. *Journal of Applied Crystallography* **2011**, *44*, 1272–1276.

(83) Troullier, N.; Martins, J. L. Efficient pseudopotentials for plane-wave calculations. *Physical Review B* **1991**, *43*, 1993–2006.

(84) Hirata, S.; Podeszwa, R.; Tobita, M.; Bartlett, R. J. Coupled-cluster singles and doubles for extended systems. *The Journal of Chemical Physics* **2004**, *120*, 2581–2592.

(85) Aprà, E. et al. NWChem: Past, present, and future. *The Journal of Chemical Physics* **2020**, *152*, 184102.

(86) Stephens, P. J.; Devlin, F. J.; Chabalowski, C. F.; Frisch, M. J. Ab Initio Calculation of Vibrational Absorption and Circular Dichroism Spectra Using Density Functional Force Fields. *The Journal of Physical Chemistry* **1994**, *98*, 11623–11627.

(87) Hamann, D. R.; Schlüter, M.; Chiang, C. Norm-Conserving Pseudopotentials. *Physical Review Letters* **1979**, *43*, 1494–1497.

(88) Fuchs, M.; Scheffler, M. Ab initio pseudopotentials for electronic structure calculations of poly-atomic systems using density-functional theory. *Computer Physics Communications* **1999**, *119*, 67–98.

(89) Louie, S. G.; Froyen, S.; Cohen, M. L. Nonlinear ionic pseudopotentials in spin-density-functional calculations. *Physical Review B* **1982**, *26*, 1738–1742.

(90) Hamann, D. R. Generalized norm-conserving pseudopotentials. *Physical Review B* **1989**, *40*, 2980–2987.

(91) Kerker, G. P. Efficient iteration scheme for self-consistent pseudopotential calculations. *Physical Review B* **1981**, *23*, 3082–3084.

(92) Bulik, I. W.; Chen, W.; Scuseria, G. E. Electron correlation in solids via density embedding theory. *The Journal of Chemical Physics* **2014**, *141*, 054113.

(93) Pham, H. Q.; Hermes, M. R.; Gagliardi, L. Periodic Electronic Structure Calculations with the Density Matrix Embedding Theory. *Journal of Chemical Theory and Computation* **2019**, *16*, 130–140.

(94) Goedecker, S. Linear scaling electronic structure methods. *Reviews of Modern Physics* **1999**, *71*, 1085–1123.

(95) Bowler, D. R.; Miyazaki, T. \mathcal{O}(N) methods in electronic structure calculations. *Reports on Progress in Physics* **2012**, *75*, 036503.

(96) Yang, W.; Wu, Q. Direct Method for Optimized Effective Potentials in Density-Functional Theory. *Physical Review Letters* **2002**, *89*.

(97) Towns, J.; Cockerill, T.; Dahan, M.; Foster, I.; Gaither, K.; Grimshaw, A.; Hazlewood, V.; Lathrop, S.; Lifka, D.; Peterson, G. D.; Roskies, R.; Scott, J. R.; Wilkins-Diehr, N. XSEDE: Accelerating Scientific Discovery. *Computing in Science & Engineering* **2014**, *16*, 62–74.

Graphical TOC Entry